NASA CR-111802

# PROPELLANT DYNAMIC PROBLEMS IN SPACE SHUTTLE VEHICLES

by
William J. Astleford
Wen-Hwa Chu
Franklin T. Dodge

FINAL REPORT, PART II
Contract No. NAS1-9890
Control No. L17-826

SwRI Project No. 02-2820

Prepared for
National Aeronautics and Space Administration
Langley Research Center
Hampton, Virginia

October 15, 1970

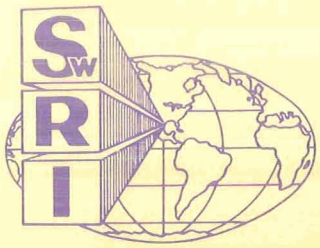


SOUTHWEST RESEARCH INSTITUTE
SAN ANTONIO HOUSTON

NASA CR-111802

SOUTHWEST RESEARCH INSTITUTE
Post Office Drawer 28510, 8500 Culebra Road
San Antonio, Texas 78228

# PROPELLANT DYNAMIC PROBLEMS IN SPACE SHUTTLE VEHICLES

by
William J. Astleford
Wen-Hwa Chu
Franklin T. Dodge

**FINAL REPORT, PART II**
**Contract No. NAS1-9890**
**Control No. L17-826**

**SwRI Project No. 02-2820**

Prepared for
**National Aeronautics and Space Administration**
**Langley Research Center**
**Hampton, Virginia**

October 15, 1970

Approved:

H. Norman Abramson, Director
Department of Mechanical Sciences

**Page intentionally left blank**

# PREFACE

This report constitutes the second of two volumes which summarize the work accomplished under Contract NAS1-9890. It contains the analysis of three fluid dynamic problems important in space shuttle design: dome impact; sloshing in tanks for which the thrust vector is not aligned with the tank axis; and hydraulic jumps in long, shallow tanks. The first part of the work, which deals with design, experiment, and analysis of a space shuttle vehicle model, is summarized in Final Report, Part I "Dynamic Interaction Between Structure and Liquid Propellants in a Space Shuttle Vehicle Model."

TABLE OF CONTENTS

LIST OF ILLUSTRATIONS

# PROPELLANT DYNAMIC PROBLEMS IN SPACE SHUTTLE VEHICLES

By William J. Astleford, Wen-Hwa Chu, Franklin T. Dodge

## INTRODUCTION

Seventy to eighty percent of the lift-off mass of proposed space shuttle vehicles consists of cryogenic liquids, and the orbiter vehicle alone will carry a larger amount of liquid into orbit than has any previous vehicle. The dynamic loads created by these large masses of liquids and the interaction of the liquid with the shuttle structure both need to be understood and accounted for in the design, a task which is greatly complicated by the nonsymmetric configuration of the shuttle, the requirement of airplane-like maneuverability, the necessity of performing safe "aborts" in the event an emergency arises during flight, and the stringent requirements imposed on structures and materials by a planned 100 re-use cycle.

A recent paper* described a number of propellant dynamic problems of shuttle vehicles for which more knowledge is required. In brief, these problems were as follows.

Slosh during ascent. --The problems of propellant slosh during thrusting are: the coupling of slosh to motions of the vehicle, and vice versa, induced by the nonaxisymmetric (side-by-side) configuration; slosh in nonaxisymmetric tanks; and sloshing in tanks when the thrust axis is not aligned with the tank axis.

Liquid motions at separation. --Large transverse impulses can cause gross liquid motions and large disturbing forces and torques at a particularly critical time.

Liquid behavior in orbit and during docking. --Low-gravity sloshing in the orbiter can occur, especially if the payload is a liquid. Docking of an orbiter containing a large mass of liquid might result in impact loads large enough to "de-latch" (i.e., abort the docking).

---

*Abramson, H. N., Dodge, F. T., and Kana, D. D., "Propellant Dynamic Problems in Space Shuttle Vehicles," Space Transportation System Technology Symposium, Vol. II - Dynamics and Aeroelasticity, pp. 59-77. NASA TM X-52876, Vol. II.

Flyback of orbiter or booster.--Any small residual mass of liquid in the tanks during a normal flyback can cause large disturbances during high angle-of-attack return or during maneuvering just prior to landing. This is because in both cases, the effective gravity is directed more or less perpendicularly to the sides of the tanks so that the liquids are contained in what are now long, shallow tanks. Liquids motions in this "bathtub" mode can be particularly pronounced.

Aborted flybacks.--If a mission is aborted, it is likely that at least a brief period of maneuvering, possibly including separation and airplane-like flying, will be necessary before the propellants can be dumped safely. If the main engines shut down during an ascent through the atmosphere, the liquids may impact on the upper bulkheads (dome impact); this can cause large disturbing forces and torques and may even rupture the tanks and cause a fireball. During separation at non-optimum heights and velocities, the liquid motions may cause serious control problems, and certainly during the flying phase of abort the large shifts in liquid c.g. would be difficult to compensate for by the pilot.

In this report, we will examine in some detail three of the problems listed above. After an unscheduled shutdown of the main engines during the atmospheric portion of the ascent, the sudden deceleration causes the propellants to move grossly toward the upper bulkheads. This liquid propellant reversal or dome impact is examined with some approximate analyses in the next section of the report, for main engine shutdown of various points along a typical ascent trajectory. Next the sloshing or wave action that occurs when the lateral acceleration of the vehicle is much greater than the axial acceleration is investigated; this "bathtub" mode of liquid response is typical of high angle-of-attack flybacks, landing, and violent separations during aborts. Finally, the sloshing of propellants in tanks for which the thrust vector is not aligned with tank is analyzed. (Unfortunately, the time schedule of this project did not allow us to carry our investigation beyond the point of determining natural frequencies.)

We have treated each of these three problems as separate and distinct in this report. Actually, there are situations such as occur in aborted missions in which all three kinds of motion are important; further research is required to elucidate the way in which one form of response is coupled to the rest.

# DOME IMPACT AND RELATED PROBLEMS

## Mathematical Development

The condition known as propellant reversal or "dome impact" results from gross reorientation of liquids in fuel tanks and is characterized by dynamic interaction forces between the arrested liquid and the tank bulkhead. The motion of the fluid is initiated by the application of transient forces or accelerations to the vehicle which have a predominant component in the direction of the tank longitudinal axis. These unbalanced loads may result from (a) an unprogrammed thrust termination of the boost engines during ascent, (b) the physical separation of the vehicles during abort and (c) the docking maneuver between the orbiter and space station.

Rigorous analytical description of the three-dimensional flow field and pressure distribution during dome impact is a formidable task. Several simplifying assumptions have been made in an attempt to obtain order of magnitude estimates of the peak impact force on the dome; these assumptions will be properly noted during the course of this development.

A nominal ascent trajectory was obtained through the cooperation of General Dynamics/Convair and used to establish flight conditions. The synthesized vehicle has a gross lift-off weight (GLOW) of 3.5 MLB and a nominal booster engine cutoff (BECO) weight of 1.28 MLB. The configuration of the vehicle is a "parallel stage" booster and orbiter; the booster has straight wings. The nonlifting trajectory has a $q_{max}$ = 560 psf at Mach number M = 1.06, staging at 212,400 ft and 9,250 fps, and a maximum axial load factor of 3.0 during the latter portion of boost. Thrust gimbal angle and vehicle angle of attack were zero for all time--hence, a gravity turn ascent. Table I summarizes system weights (including orbiter), volume and weight of fuel on board at selected times, the drag-to-weight ratio, dynamic pressure, etc. Fuel weight-volume calculations were based on the assumption that no residuals remain in the boost tanks at nominal BECO and that there was one tank for each propellant constituent. The drag values do not reflect the decrease in base pressure resulting from engine shutdown.

Broadly, the approach to the dome impact problem is as follows. Three points were selected for an impact analysis of the booster tanks: t = 50, 70, and 136 sec into the mission for LH2 impact and t = 50, 70, and 110 sec for LOX impact. These times fall within the extremely critical abort Mode IB (20 to 140 seconds) as defined by the NASA-SSV predesign study of Reference 1. The final times differ, as will be discussed later, because the LOX volume remaining at t = 136 sec was incompatible with the analysis. This situation will be clarified later. At each of the selected points prior to assumed thrust termination the trajectory performance parameters

TABLE I. --(NOMINAL) SSV ASCENT TRAJECTORY PARAMETERS

| t(sec) | Mach No. | $W_s$(MLB) | $W_{LOX}$(MLB) | $W_{LH2}$(MLB) | $V_{LOX}(ft^3)$ | $V_{LH2}(ft^3)$ | D/W | q(psf) | n |
|---|---|---|---|---|---|---|---|---|---|
| 50 | .81 | 2.87 | 1.36 | .226 | 18,200 | 51,250 | .153 | 476 | 1.66 |
| 70 | 1.34 | 2.62 | 1.14 | .190 | 15,300 | 43,000 | .423 | 556 | 1.65 |
| 110 | 3.10 | 2.11 | .71 | .119 | 9.530 | 26,800 | .203 | 239 | 2.43 |
| 136 | 4.77 | 1.79 | .43 | .072 | 5,750 | 16,250 | .0904 | 89 | 3.00 |

| | | |
|---|---|---|
| t | = | time after lift-off |
| $W_s$ | = | total system weight |
| GLOW | = | 3.5 MLB |
| $W_{BECO}$ | = | 1.28 MLB |
| O/F | = | 6:1 |
| $\rho$LOX | = | 74.8 $lb/ft^3$ |
| $\rho$LH2 | = | 4.42 $lb/ft^3$ |
| $V_{stage}$ | = | 9,250 ft/sec |
| $h_{stage}$ | = | 212,400 ft |
| n | = | total axial load factor |

permitted calculation of the axial and transverse components of the total load factor vector, $\bar{n}$, as well as the quiescent fuel free surface angle which is taken to be normal to that load factor. Figure 1 presents the coordinate system and summarizes the definition of load factor and fuel free surface angle, $\beta$. The trajectory which was furnished to us was non-lifting with zero angle of attack and zero thrust gimbal angle. Consequently, the load factor is purely axial and the fuel surface angle is idealistically zero.

Thrust termination is assumed to take place instantaneously rather than following a throttling schedule similar to that encountered during initiation of nominal staging procedures. Therefore, immediately following termination, the vehicle encounters a deceleration field of a magnitude equivalent to the drag-to-weight ratio. Alternately, the liquids react to an acceleration field of the same magnitude which is assumed to act in a step function fashion. The drag force is assumed to remain constant during the brief period of time from thrust termination to dome impact.

With the theoretical fuel free surface angle and acceleration field defined, tank sizing and liquid equations of motion can now be considered. The booster LH2 tank was taken to be a hemispherically-capped right circular cylinder as shown in a general orientation in Figure 2. Consistent with NASA and other Phase A predesigns; the tank longitudinal axis is parallel to the booster reference axis, and the tank diameter, $d_t$, of 30 ft is representative of these design layouts. Neglecting ullage volume, i.e. the tank is completely full at launch, the cylinder length is sized according to Equations (1) and (2) for a 6:1 oxidizer-to-fuel ratio. The volume of fuel remaining in the LH2 tank at any time, t, is calculated by substituting the appropriate W(t) from the trajectory for the GLOW in Equation 1. By using Equation (3) the liquid free surface is located longitudinally relative to the tank fixed x-y axes. The rationale behind inclusion of non-zero fuel surface angles in the analysis will be clarified in the next section. Upon thrust termination a particle of liquid, $m_l$, will be accelerated toward the dome at, conservatively, D/W g's, where W is the total system weight. Assuming that there is initially no interaction between fluid particles or between the fluid and the tank walls, the motion of the leading edge of fluid relative to tank fixed axes is governed, according to Reference 2, by Equations (4), (5), and (6). Straightforward solution of these equations permits calculation of time of arrival, $t_o$, and velocity $\dot{y}(t_o)$ of the first particle of fluid to reach $y = L_c$, Equation (7). The liquid is assumed to traverse the contour of the hemispherical dome in a curved sheet with an unattenuated velocity, $\dot{y}(t_o)$. The peak impact force was taken to be the steady state contribution to the one-dimensional momentum theorem, and the unsteady term, which was neglected, reflected a lower level transient

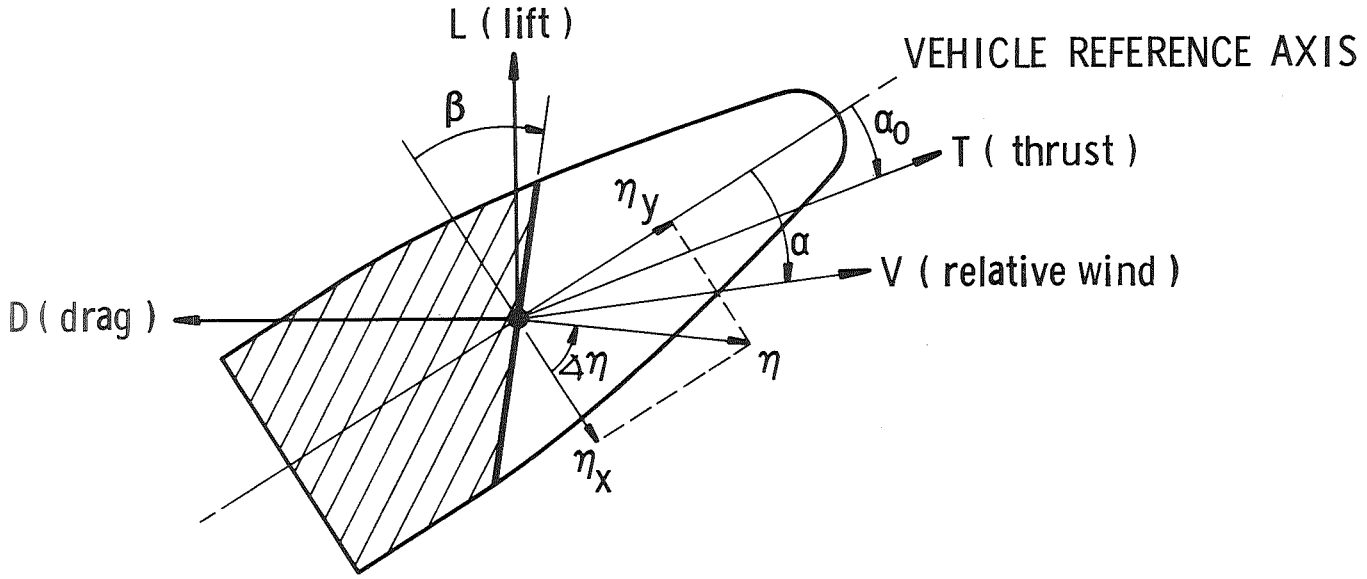


$$\eta_x = \frac{-L\cos\alpha - D\sin\alpha + T\sin\alpha_0}{W}$$

$$\eta_y = \frac{-L\sin\alpha - D\cos\alpha + T\cos\alpha_0}{W}$$

$$\Delta\eta = 90^\circ - \beta = \arctan\frac{\eta_y}{\eta_x}$$

3040

FIGURE 1. --DEFINITIONS OF VEHICLE LOAD FACTOR AND FUEL SURFACE ANGLE

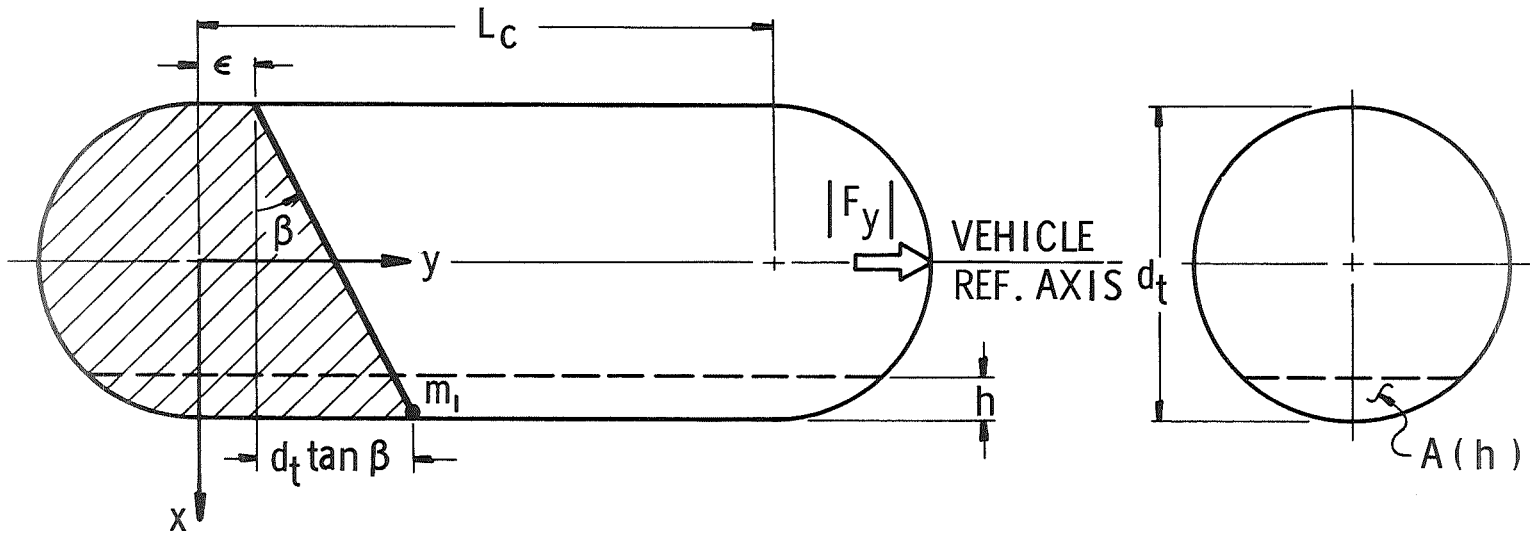


h = Static settling depth

$$\mathcal{V}_{LH_2\,TANK} = \frac{1}{7}\,(GLOW - W_{BECO})/\rho_{LH_2} \qquad (1)$$

$$L_C = \left[\mathcal{V}_{LH_2\,TANK} - \frac{4}{3}\pi\left(\frac{d_t}{2}\right)^3\right]/\frac{\pi}{4}d_t^2 \qquad (2)$$

$$\mathcal{V}_{LH_2} = \frac{\pi}{8}d_t^3\left(\tan\beta + \frac{2}{3}\right) + \frac{\pi}{4}d_t^2\,\epsilon \qquad (3)$$

$$\ddot{y}(t) = \left(\frac{D}{W}\right)g \qquad (4)$$

$$\dot{y}(0) = 0 \qquad (5)$$

$$y(0) = \epsilon + d\,\tan\beta \qquad (6)$$

$$\dot{y}(t_0) = \left(\frac{D}{W}\right)g\left\{\frac{2\left[L_C - (\epsilon + d_t\tan\beta)\right]}{(D/W)g}\right\}^{1/2} \qquad (7)$$

$$|F_y| = 2\rho_{LH_2}A(h)\left[\dot{y}(t_0)\right]^2 \qquad (8)$$

3041

FIGURE 2.--LIQUID HYDROGEN TANK CONFIGURATION AND EQUATIONS

force associated with the initial entry of fluid into the dome.* The steady state force of the fuel on the dome is described by Equation (8). It has been tacitly assumed that the quiescent mode of slosh does not occur. To fully apply Equation (8) the "effective nozzle area," A(h), must be evaluated. This area is taken to be the cross-sectional area of the fuel sector at $y = L_c$ which corresponds to the static, transverse settling depth, h, consistent with the volume of liquid in the tank at thrust termination. The depth and area in question are shown schematically in Figure 2. The iterative solution for A(h) is easily obtained using the tables of areas and heights for sectors and segments of circles and spheres in Reference 3. Ideally, the line of action of the calculated force coincides with the tank longitudinal axis. In reality, however, the reaction force will be inclined at some small angle to this axis and will be slightly larger than calculated due to neglect of the lateral movement of the fuel center of gravity during modal slosh. These latter effects, however, should be considered minimal from an order of magnitude viewpoint.

The procedures for evaluating LOX dome impact follow lines of development similar to those used for LH2 dome impact. The basic difference is the LOX tank shape and orientation with respect to the vehicle reference axis. As suggested by two Phase A preliminary design brochures, the LOX tank configuration on the booster was taken to be a frustum of a right circular cone, capped at both ends by hemispherical shells without regard for points of tangency. The LOX tank generally lies forward of the LH2 tank, and, due to packaging constraints, the tank axis is inclined to the vehicle reference axis by an angle, $\phi$, with the smaller hemispherical end pointing generally forward. Figure 3 illustrates this tank in a general orientation. Frustum length and cone half angle were calculated using Equations (9), (10), and (11). After calculating the LOX volume remaining in the tank at time, t, in a manner analogous to the LH2 volume calculations, the LOX free surface is located using Equation (12), thus defining h, $\Delta h$ and d. From predesign scale drawings of the LOX tank the angle, $\phi$, is expected to be small enough to permit approximation (12b) to be imposed. The drag-to-weight ratio was then resolved into components in the direction of the slant axes, $X_1$ and $Y_1$, where it was assumed that upon thrust termination, particle $m_1$ was acted upon only by the $Y_1$ component of D/W, thus giving rise to Equation 13. The velocity and time of arrival of $m_1$ at $Y_1 = L/\cos\theta$ are determined in a manner similar to the corresponding LH2 calculation. Equation (16) describes the impact force, $|F_y|$. The effective nozzle area is again taken to be the transverse, settled, fuel cross-sectional area at the entrance to the smaller dome (at section $A_2$) subject to the constraint of remaining LOX volume on board at thrust termination. The iterative

*After the conclusion of the research reported herein, the NASA technical monitors brought to our attention some unpublished notes by Larry D. Pinson, dated November 27, 1963, in which a similar analysis is outlined.

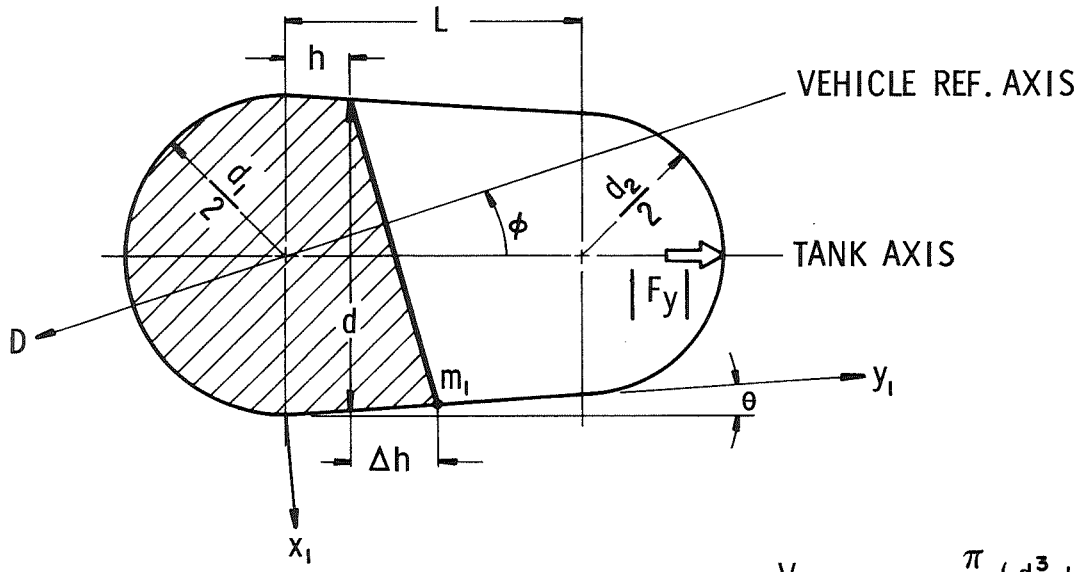


$$V_{LOX\ TANK} = \frac{6}{7}\left(GLOW - W_{BECO}\right)/\rho_{LOX} \qquad (9)$$

$$L = \frac{V_{LOX\ TANK} - \frac{\pi}{12}\left(d_1^3 + d_2^3\right)}{\frac{\pi}{16}\left[\left(d_1 + d_2\right)^2 + \frac{1}{3}\left(d_1 - d_2\right)^2\right]} \qquad (10)$$

$$\theta = \text{ARCTAN}\left(\frac{d_1 - d_2}{2L}\right) \qquad (11)$$

$$V_{LOX} = \frac{1}{12}\pi d^3 + \frac{1}{12}\pi h\left[d^2 + d_1 d + d^2\right] + \frac{1}{8}\pi d^2 \Delta h \qquad \text{TAN}\ \phi \approx \frac{\Delta h}{d} \qquad \text{TAN}\ \theta = \frac{d_1 - d}{2h} \qquad (12)$$

$$\ddot{y}_1(0) = \left(\frac{D}{W}\right) g\ \cos(\theta - \phi) \qquad (13)$$

$$\dot{y}(0) = 0 \qquad (14)$$

$$y_1(0) = \frac{h + \Delta h}{\cos\theta} \qquad (15)$$

$$\left|F_y\right| = 2\rho_{LOX} A_2 \left[\dot{y}(t_o)\right] \qquad (16)$$

$$V_{SEG.\ FRUST} = \frac{1}{6} L\left[A_1 + A_2 + 4A_M\right] \qquad (17)$$

3042

FIGURE 3.--LOX TANK CONFIGURATION AND GOVERNING EQUATIONS

procedure requires the use of the "prismoidal formula," Equation (17), for the LOX volume in a segment of a cone frustum. $A_1$ and $A_2$ are the fuel areas at $d_1$ and $d_2$, respectively, while $A_M$ is the fuel area at L/2.

To summarize this section, an approximate method has been developed to obtain order of magnitude estimates of the maximum dome impact force of LOX and LH2 resulting from impromptu termination of thrust on the main booster engines. The LH2 analysis incorporates the ability to investigate the sensitivity of impact force to small non-zero free surface angles, which might arise as a result of a combination of vehicle lift component, positive angle of attack and non-zero thrust gimbal angle. The LOX analysis permits the tank offset angle to be treated as an independent variable for design purposes. In both cases the impact forces act along the appropriate tank axis.

## Liquid Hydrogen Dome Impact During Boost

The development outlined previously was applied to the impact of LH2 into the forward dome of the booster fuel tank for thrust termination at the previously indicated times, and the results of the principal calculations have been summarized in Table II. The t = 70 sec point corresponds to nearly a $q_{max}$ condition (within 5 psf) on a nominal outbound trajectory while the t = 136 sec point occurs at the onset of a boost engine throttle sequence designed to limit total load factor to 3 g's. It should be noted that even though the fuel level becomes progressively lower as time from lift-off increases, the arrival time, $t_o$, at the dome entrance does not increase correspondingly due to the nature of the drag-to-weight profile. The variation of entrance velocity follows, qualitatively, from similar lines of reasoning.

The magnitude of the LH2 impact force is shown in Figure 4. As expected, the most severe impact occurs in the vicinity of $q_{max}$ or the drag pinch point. In general, the variation of calculated impact force with time follows the same trend as the variation of aerodynamic load factor, D/W. Also shown in Figure 4 is the sensitivity of the dome impact force at $q_{max}$ to non-zero fuel free surface angles. A moderate dependence is indicated--approximately 870 lb/degree of surface angle. This sensitivity was calculated to provide an engineering feel for the manner in which the impact force would change as a result of the following assumptions and constraints imposed on the analysis:

(1) The flat, non-rotating earth assumption of Reference 2, which was used in this analysis to calculate the fuel free surface angle, implies the omission of acceleration terms from the trajectory differential equations that result in incremental fuel surface angles of the order of 1° at $q_{max}$ and 3° at the onset of the 3g throttle.

TABLE II. --SUMMARY OF LH2 TANK CONDITIONS

| $t \sim$ sec | $\beta \sim {}^{o}$ | $\epsilon \sim$ ft | $t_o \sim$ sec | $\dot{y}(t_o) \sim$ fps | $A(h) \sim ft^2$ | $h \sim$ ft |
|---|---|---|---|---|---|---|
| 50 | 0 | 63.4 | 2.35 | 11.6 | 530 | 21 |
| 70 | 0 | 50.9 | 1.96 | 26.6 | 444 | 18 |
| ↓ | 5 | 49.6 | 1.91 | 25.8 | ↓ | ↓ |
| | 10 | 48.3 | 1.86 | 25.2 | | |
| | 15 | 46.9 | 1.80 | 24.5 | | |
| 136 | 0 | 13.0 | 6.64 | 19.3 | 178 | 9 |

$L_c$ = 77 ft

$d_t$ = 30 ft

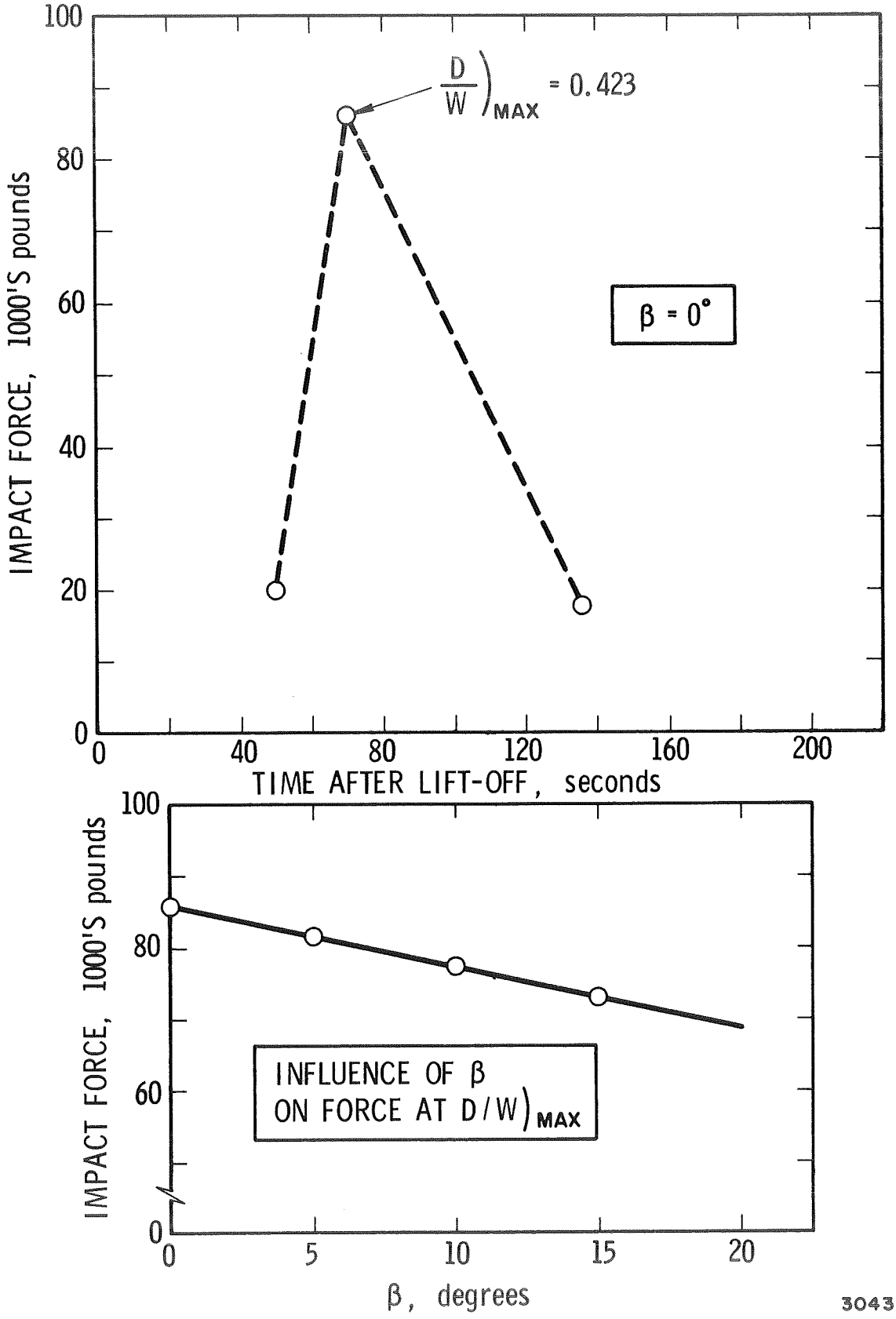


FIGURE 4.--LH2 DOME IMPACT, THRUST TERMINATION DURING BOOST

(2) The assumption of a nonlifting, zero angle of attack trajectory, which resulted in zero fuel surface angles, does not appear to be totally valid for other shuttle designs incorporating a more conventional aircraft-type booster.

(3) In all likelihood a thrust termination would actuate the attitude control system in an attempt to maintain vehicle stability. Control surface deflections as well as pitching moments from an RCS would result in non-zero fuel surface angles at the initiation of the slosh motion.

Some discussion of the impact magnitude is needed in light of the "effective nozzle areas" and fuel depths used to calculate the forces. Both the 50 and 70 sec thrust termination times result in static settling depths that exceed the radius of the tank with only the 3g condition near the end of boost producing a depth less than 15 ft. Obviously it is impossible, in the strictest sense, for the LH2 to execute full sheet flow at t = 50 and 70 sec as has been postulated. Therefore, some reduction in peak impact force might realistically be expected. If the "effective nozzle area" at $q_{max}$ were to be reduced by approximately 25 percent (equivalent fuel depth of 15 ft), the impact force would be reduced only to about 69,000 lb. Hence, the order of magnitude of the estimates are quite reasonable. A different perspective can be gained by looking at the induced tensile stress at the hemisphere--cylinder intersection. The average stress in the wall is simply the impact force divided by the annular tank area. For a tank wall thickness of 0.1 in., the resultant stress is 764 psi at $q_{max}$. This stress level is well below the elastic limit of aluminum, and structural damage seems remote at these levels for the LH2 tank.

## Liquid Oxygen Dome Impact During Boost

The counterparts of Table II and Figure 4 are presented in Table II and Figure 5 for the dome impact of LOX in the booster. In this case the third analysis point was reduced from t = 136 sec to t = 110 sec because the former time resulted in an on-board LOX volume at thrust termination that yielded in a negative oxidizer settling depth measured with respect to the junction of the cone frustum and forward hemispherical dome. In Figure 5 we observe that the basic trends are the same for both LOX and LH2 impact except that the LOX force level is significantly larger. This magnification of the force is directly attributable to the 17:1 LOX:LH2 mass density ratio and is inversely related to the ratio of LH2 to LOX effective nozzle areas.

It was pointed out earlier that, due to packaging constraints, several system designs require a tank offset angle, $\phi$. In addition, most designs position this tank well forward of the vehicle center of gravity, and the nose of the tank is canted downward with respect to the vehicle reference line.

TABLE III. --SUMMARY OF LOX TANK CONDITIONS

| t ~ sec | $\phi$ ~ $^{o}$ | $y_1(0)^*$ ~ ft | $t_o$ ~ sec | $\dot{y}(t_o)$ ~ fps | $A_2$ ~ $ft^2$ | Fuel Depth at $A_2$ |
|---|---|---|---|---|---|---|
| 50 | 0 | 20.8 | 2.84 | 13.7 | 154 | 12.2 |
| 70 | 0 | 14.10 | 1.98 | 26.5 | 124 | 9.9 |
| ↓ | 5 | 15.5 | 1.91 | 25.8 | ↓ | ↓ |
| | 10 | 16.30 | 1.88 | 25.5 | | |
| | 15 | 17.4 | 1.83 | 24.9 | | |
| 110 | 0 | 3.73 | 3.34 | 21.4 | 59 | 5.5 |

$$^*y_1(0) = \frac{h+\Delta h}{\cos\theta}$$

$L = 39.7$ ft

$d_1 = 30$ ft

$d_2 = 15$ ft

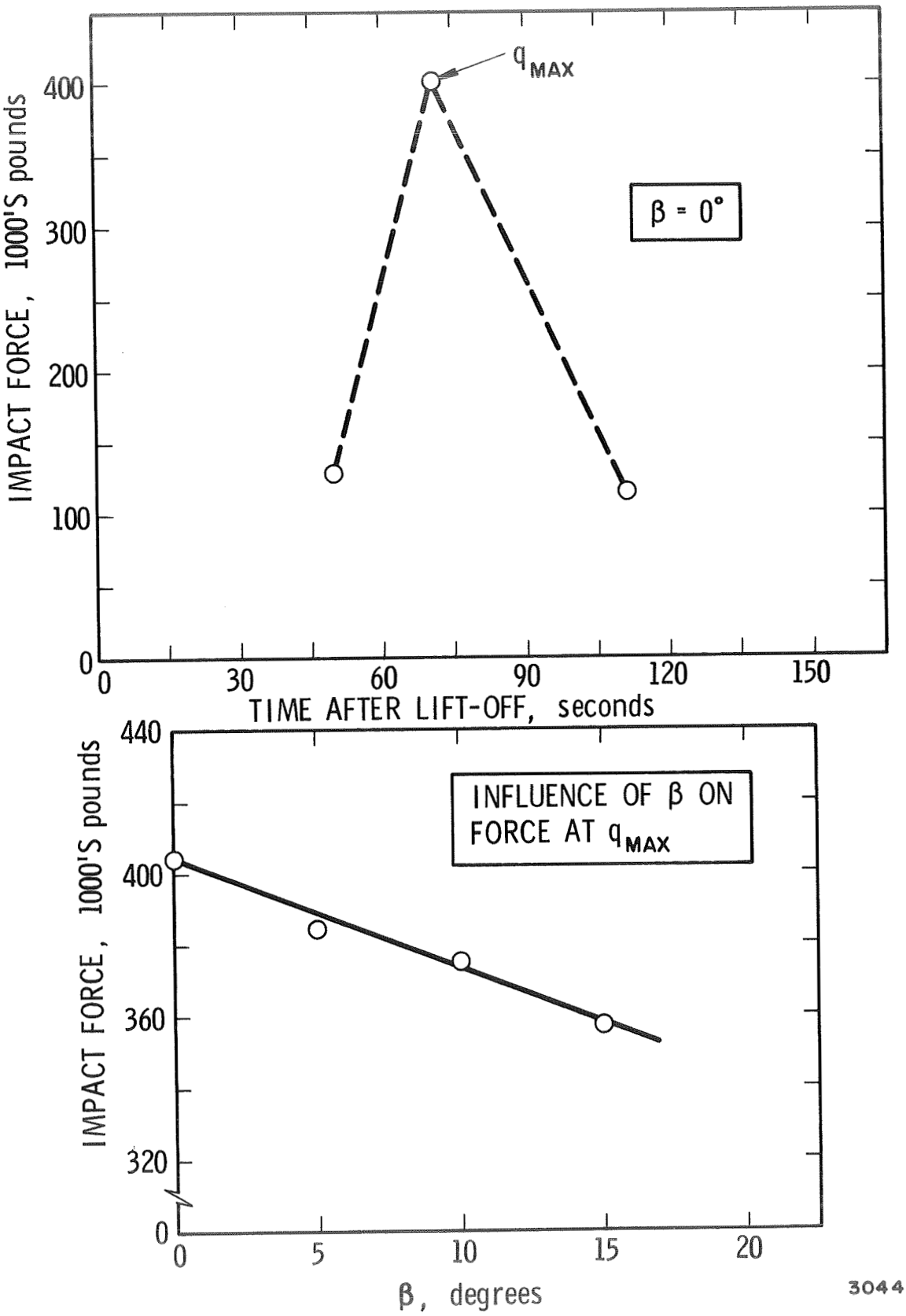


FIGURE 5.--LOX DOME IMPACT, THRUST TERMINATION DURING BOOST

This situation is desirable from a control system standpoint because the impact force vector, which is aligned with the tank axis, contains a lateral component, normal to the vehicle axis, that will produce a stabilizing, nose down pitching moment upon thrust termination which should assist in overcoming the inherent instability of the booster during separation.

For a tank with a wall thickness of 0.1 in., the longitudinal stress at the forward bulkhead juncture is of the order of 7000 psi for a $q_{max}$ thrust termination and represents approximately 10 percent of the yield strength of a typical high strength aluminum.

## Dome Impact During Abort Separation at $q_{max}$

We have previously estimated the propellant reversal force resulting from a thrust termination of the main booster engines at a $q_{max}$ condition, and now we will consider the propellant reversal associated with forces on the booster caused by physical separation of the orbiter and booster at zero angle of attack. Several types of forces may be involved. The first force encountered is due to mechanical or propulsive separation of the two vehicles which is designed to impart a relative acceleration between the orbiter and booster. As the vehicles separate, their individual shock wave flow fields interact inducing the second class of loads--large aerodynamic interference loads. The third class of loads results from impingement of the orbiter main engine exhaust plume on the aft portion of the booster. Finally, since abort implies a non-optimum staging point, the booster may be required to generate negative lift in order to maintain stability and avoid collision with the orbiter.

In general, the above loads are heavily dependent on vehicle configuration and flight regime. In the absence of firm estimates for their individual contributions to the separation dynamics, we may consider their aggregate effect in a parametric fashion. To this end, during separation the booster is assumed to be acted upon by the basic zero-lift drag force at $q_{max}$ plus a resultant separation force, R acting at an angle, $\delta$, to the booster reference line as illustrated in Figure 6. R includes the contribution of the separation forces over and above the basic drag at zero lift. The orientation of the force vector, R, is based on the experimental results of Reference 4. Separation at Mach 3.0 and booster angles of attack less than 8° induced a negative normal force coefficient and a positive axial force coefficient on the booster, thus producing a resultant force coefficient in the direction of R. We assumed that this behavior can be extrapolated to transonic speeds with the general orientation remaining unaltered. Dome impact of propellants in the orbiter stage should be minimal considering that the tanks are full at this time; therefore, the effect of separation forces on the orbiter will not be considered.

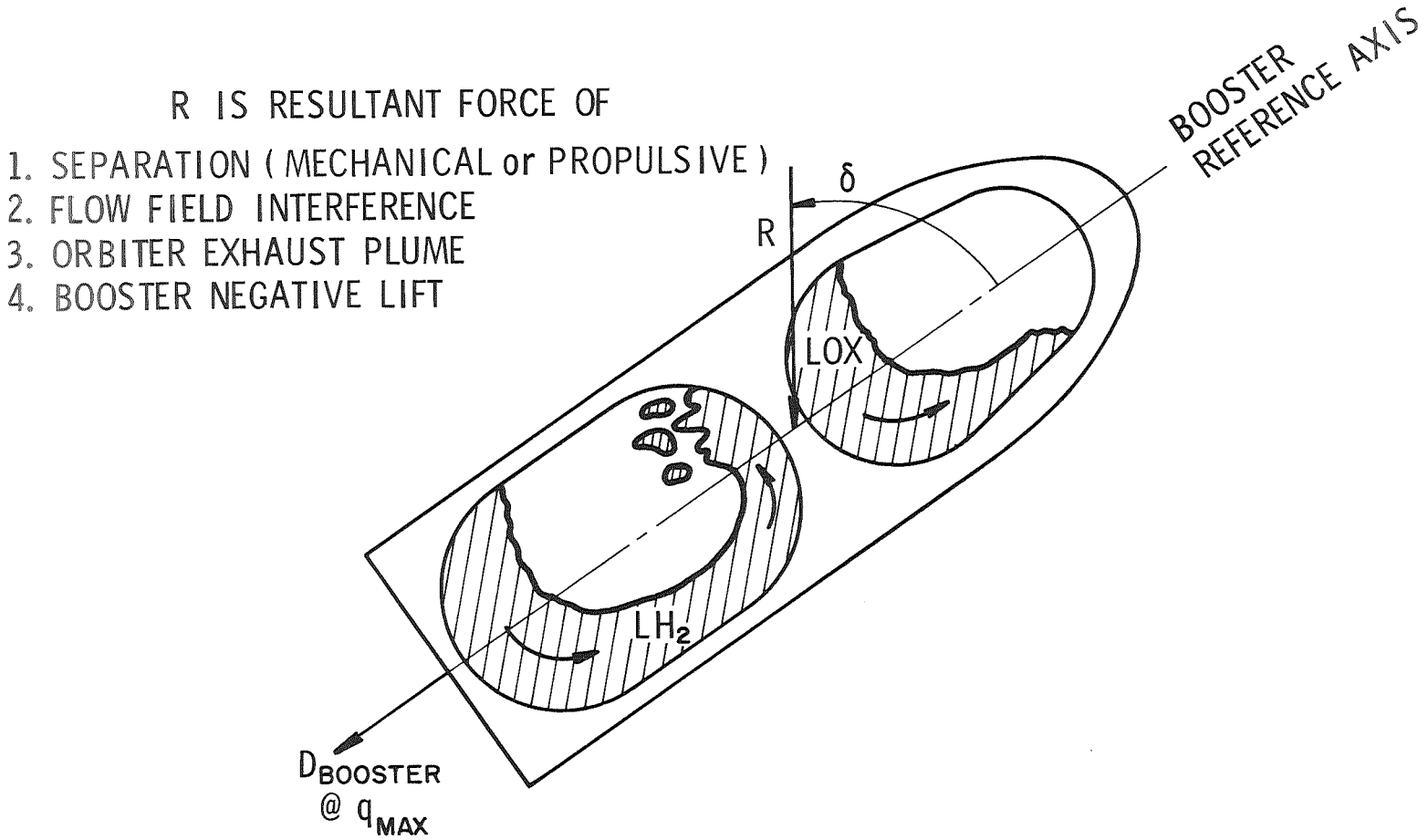


FIGURE 6. --IDEALIZED BOOSTER ABORT FORCE FIELD

Wind tunnel abort separation studies presented at the recent Symposium on Space Transportation Systems (ref. 5) were directed at vehicle separation at free stream Mach numbers in excess of 3.0. However, there appears to be negligible experimental abort data available when $q_{max}$ occurs transonically as it does for the ascent trajectory under consideration. However, test data for the damping-in-pitch derivative of a single blunted cone-cylinder-flare body indicates a highly unstable transonic behavior should be anticipated (ref. 6).

Propellant motions initiated by thrust termination will probably not have time to subside before being acted upon by the various components of R. This situation implies that the initial conditions on fluid motion postulated previously are not valid. However, for the lack of quantitative information regarding the fluid motion and orientation at separation with which to form new initial conditions, we assume that the preseparation disturbances have diminished to the point where a quiescent surface exists. The separation causes acceleration of the propellants toward their respective domes with a magnitude:

$$\ddot{y}(0^-) = \begin{cases} \left[\left(\frac{D}{W}\right)_{Booster} + \frac{R\cos\delta}{W_{Booster}}\right] g & , \quad LH2 \\ \left[\left(\frac{D}{W}\right)_{Booster} + \frac{R\cos\delta}{W_{Booster}}\right] g\cos(\theta - \phi) & , \quad LOX \end{cases}$$

The term containing the separation forces is considered an independent variable. The drag-to-weight ratio in the previous equations represents a condition where the vehicle base is partially filled with exhaust plume gases. Accordingly, when the thrust is terminated base drag increases; to account for this situation the LOX dome impact force was also calculated for an increase of 20% in D/W. A 20% decrease in D/W was also considered in an attempt to simulate a booster configuration with a different drag profile.

In Figures 7 and 8 the impact force per unit "effective nozzle area" is presented as a function of the axial component of the resultant separation force, R, up to 6 g's. The impact force is represented in this manner because of the inadequacy of applying the previous nozzle areas due to the unknown orientation of the propellants during separation. As can be seen the steady state impact force is heavily dependent on the separation induced axial "g" level regardless of the assumption on nozzle area and is relatively insensitive to variations in booster zero-lift drag. The addition of a 1g increment in axial separation force results approximately in a trebling of the impact force over the pure thrust termination case, which corresponds to R = 0. Hence, from the standpoint of structural damage to the tank and controllability due to movement of fuel center of gravity and fuel angular momentum, the impact

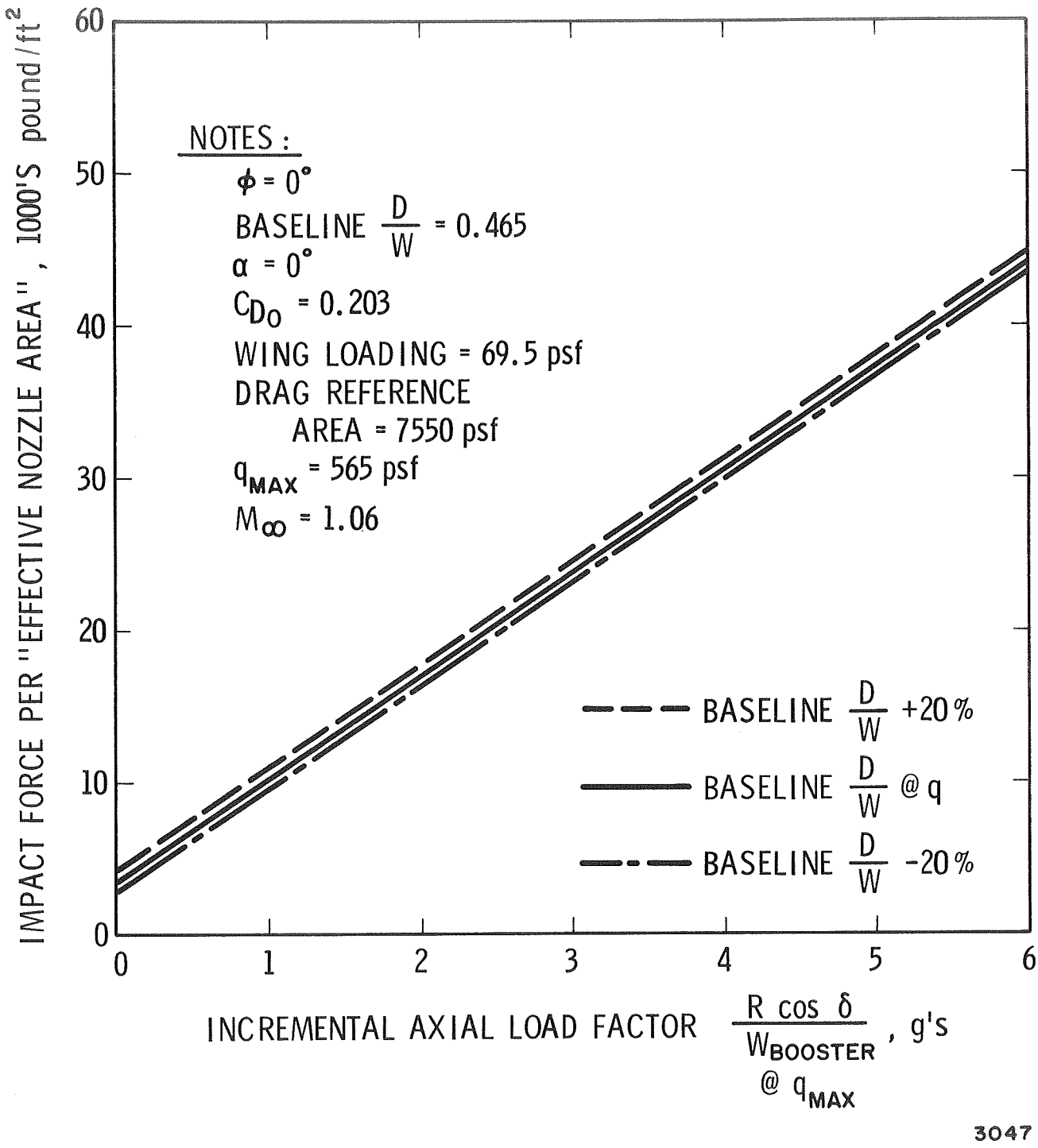


FIGURE 7.--LOX DOME IMPACT FORCE PER UNIT "NOZZLE AREA" FOR ABORT SEPARATION AT $q_{max}$

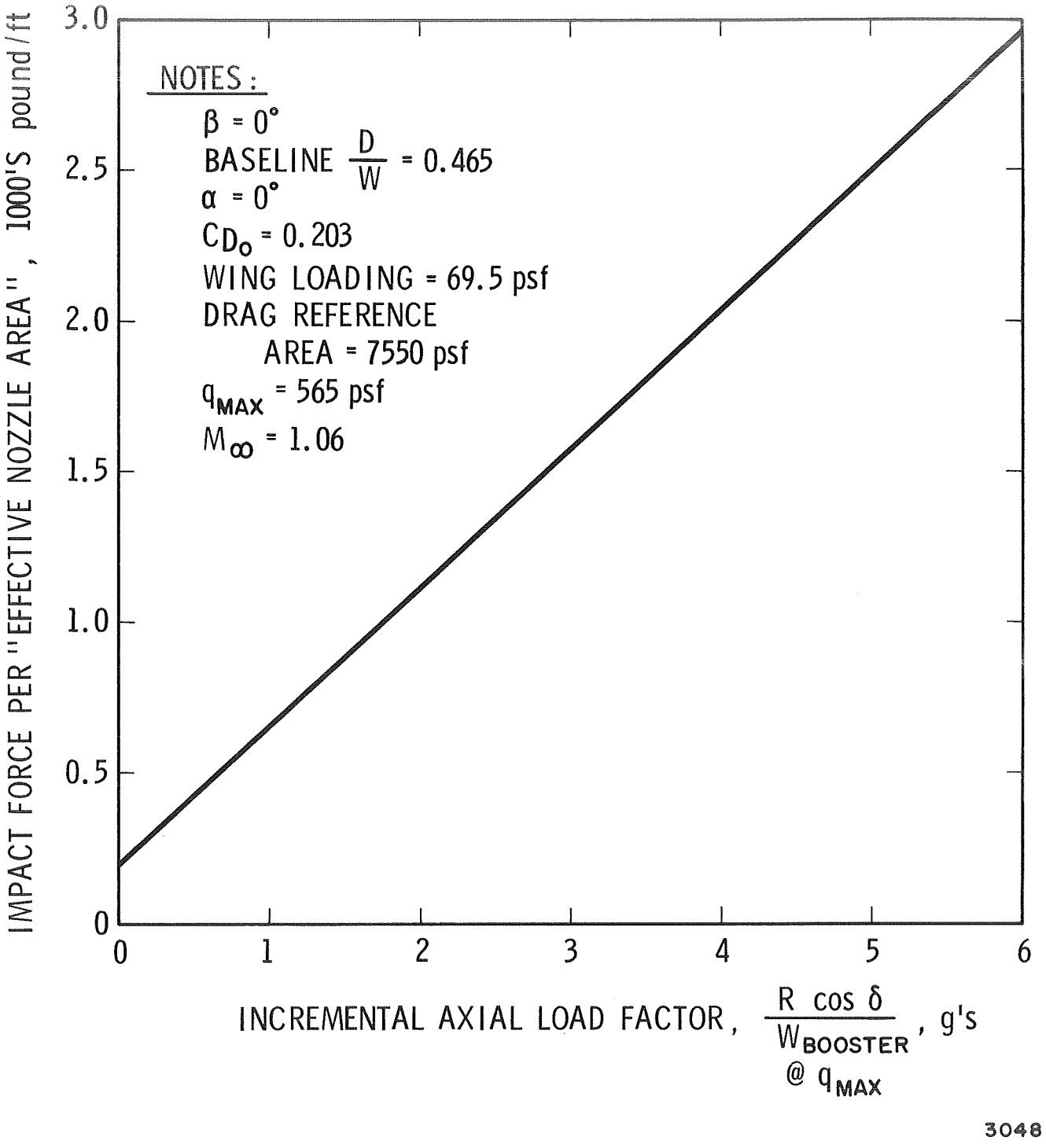


FIGURE 8.--LH2 DOME IMPACT FORCE PER UNIT "NOZZLE AREA" FOR ABORT SEPARATION AT $q_{max}$

forces during separation at a transonic $q_{max}$ are more severe than at any other point on the outbound trajectory.

## Docking Dome Impact

The turning vane analysis used for the previous cases was adopted to investigate the dome impact resulting from fuel movements during docking of the orbiter and space station. Experience gained from the first stage boost studies suggests that the principal loads are associated with movements of LOX. Therefore, it was assumed that the forces which would significantly affect the ACS (attitude control system) result from dome impact of an assumed 1% LOX reserve in the main orbiter boost tanks which is carried to TPI. It was further assumed that the LOX/LH2 remaining after OMS (orbital maneuver system) burn would result in minimal fuel induced loads on docking.

The LOX tank configuration was taken to be a hemispherically capped cylinder whose longitudinal axis is collinear with the vehicle reference and docking axes, i.e., no misalignment. The tank diameter, which was assumed to be 20 ft, agrees quite closely with the Phase A designs and is only slightly larger than the NASA DC-3 predesign. Sizing of tank length is determined by the boost LOX requirements which will be considered subsequently.

In a low gravity environment the fuel free surface assumes a minimum potential energy configuration. For the case under consideration this surface is hemispherical, being concave toward the empty portion of the tank. As such it was felt that the modal form of slosh during docking was more probabilistic than the quiescent mode.

The docking maneuver itself was considered to take place under coasting or non-thrusting conditions with a closure rate, $\Delta v_c$, ranging from 1 to 3 fps. A momentum balance for an inelastic docking is approximately

$$M(\Delta v_c) = m_f(\Delta v_c) + \int_{t_1}^{t_2} F\,dt$$

where M and $m_f$ are the orbiter total mass and fuel mass, respectively. The left side of the above equation represents the orbiter momentum with respect to the space station, and the integral signifies the impulse resulting from initial contact between the two structures. The momentum of the fuel is manifested in the dome impact force. Regardless of the amount of fuel in a tank a particle on the free surface will not reach the turning vane with a velocity greater than the closure velocity, $\Delta v_c$. This situation is particularly true if surface tension and viscous forces are considered.

LOX tank sizing was accomplished as follows. A nominal General Dynamics orbiter requires 510,400 lb of LOX/LH2 to boost the second stage from separation to insertion in a 51 X 100 n.m. orbit. Assuming a 6:1 oxidizer-to-fuel ratio and a 1% reserve, second stage boost requires 441,000 lb of boost LOX and occupies 5,900 $ft^3$ of tank volume. Proceeding as though the LOX completely fills the tank (neglect volume required for application of ullage pressure), the cylindrical section was calculated to be 5.45 ft long.

The 1% baseline reserve volume of 59 $ft^3$ has a settling depth, h, of 1.4 ft and an "effective nozzle area" of 9.75 $ft^2$. The force equation was applied to this configuration, as well as to a ±10% variation of residual LOX about the baseline, and the results are shown in Figure 9.

While a 3 ft/sec closure rate probably represents an extreme closure rate, it is apparent that the impact forces sustained by the dome are not extraordinarily large. The docking simulation tests conducted in Reference 7 utilized a 1 ft/sec closure rate. For closure rates of less than 2 ft/sec, forces are relatively insensitive to variations of residual LOX volume. It is doubtful that these force levels will have structural damage implications; however, they should be of value in assessing control system requirements.

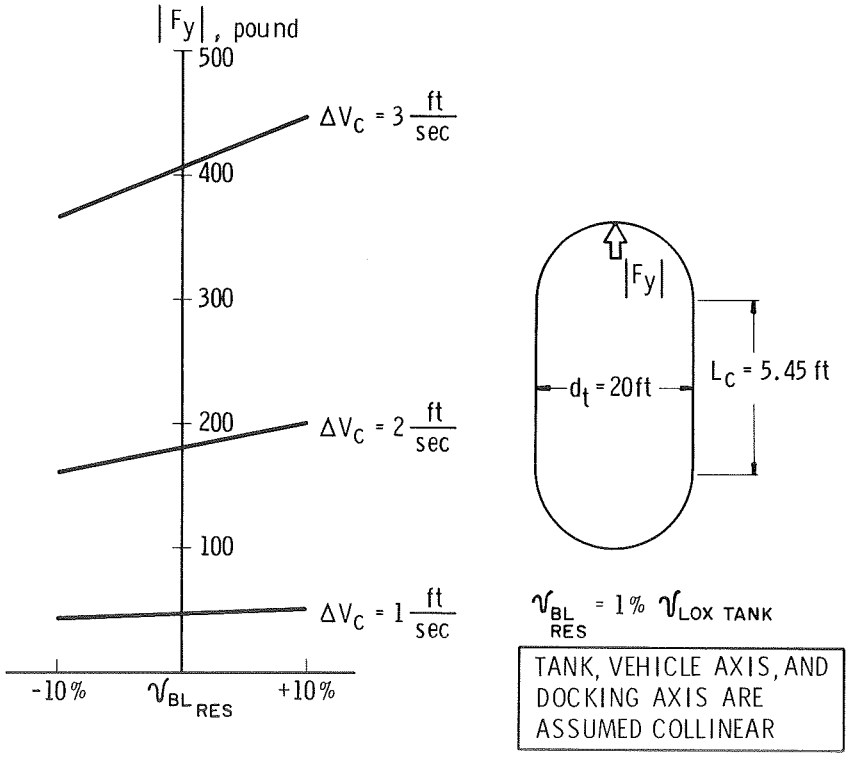


FIGURE 9.--SENSITIVITY OF LOX DOME IMPACT FORCES DURING DOCKING TO LOX FUEL RESERVES IN ORBITER BOOST TANK

## References

1. DC 3--Space Shuttle Study. vol. I and II, NASA Manned Spacecraft Center, April, 1970.

2. Dalzell, J. F.: Liquid Impact on Tank Bulkheads. Chapter 10, The Dynamic Behavior of Liquids in Moving Containers. NASA SP-106, 1966.

3. Marks, L. S.: Mechanical Engineering Handbook. McGraw-Hill Book Company, Inc., 1951.

4. Decker, J. P.: An Exploratory Experimental and Analytical Study of Separating Two Parallel Lifting Stages of a Reusable Launch Vehicle at Mach Numbers of 3 and 5. Masters Degree Thesis, University of Virginia, May 1968.

5. Decker, J. P., et al.: Abort Separation Including Aerodynamic, Dynamic and Trajectory Influences. NASA TM X-52876, July, 1970.

6. Orlik-Ruckemann, K. J.: Possible Use of Half-Model Oscillatory Techniques for the Study of Shuttle Abort Separation Dynamics. NASA TM X-52876, July, 1970.

7. Siller, J. F.: Full Scale Apollo Docking Simulation Tests. Journal of Spacecraft. vol. 7, No. 8, Aug. 1970.

# LIQUID OSCILLATIONS IN LONG, SHALLOW TANKS

## Introduction

During a normal orbiter or booster flyback trajectory, there are times when the angle-of-attack and load factors are such that the "effective" gravity, $g_{eff}$, is nearly perpendicular to the propellant tank walls. For example, this situation occurs in the General Dynamics/Convair booster reentry during the period from about 40 seconds after staging to about 100 seconds after staging; and, of course, during the landing, gravity is always oriented nearly perpendicular to the tank walls. If any residual propellant remains in the tank during these times, as is likely because of incomplete venting (this is certain to occur during an abort before staging), the propellant is contained in tanks that are now long and shallow; this is shown schematically in Figure 10.

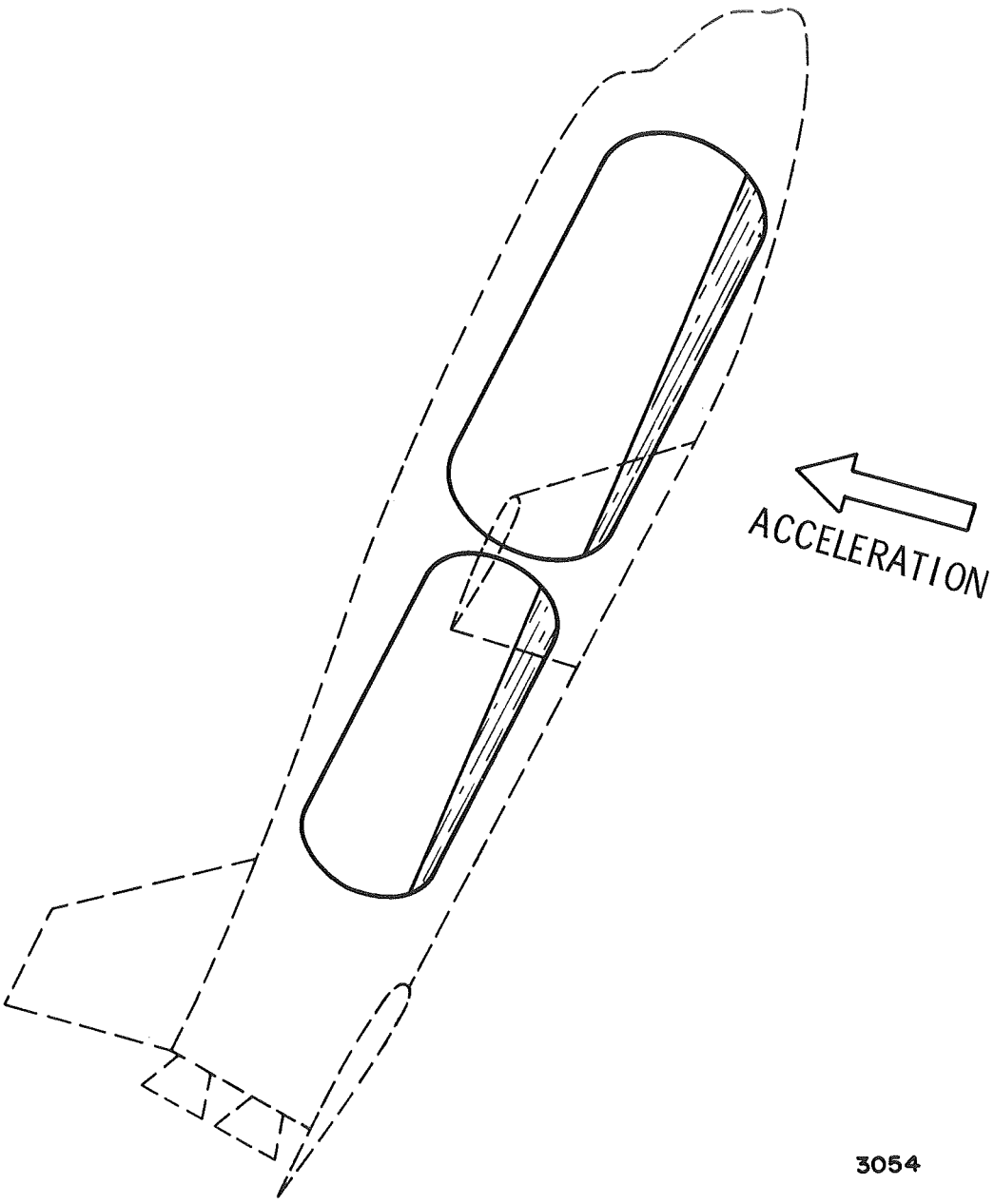


FIGURE 10.--RESIDUAL PROPELLANT LOCATION DURING HIGH ANGLE-OF-ATTACK FLYBACK

When the length of the tank is large with respect to the depth of the liquid, two kinds of liquid free-surface oscillations can occur (ref. 1, 2). If the tank oscillation frequency is not too close to the "slosh" frequency (or if the disturbance is not periodic), standing waves will appear on the surface. This response can be analyzed by linearized theories, and a mathematically equivalent mechanical model can be used to predict the forces and moments exerted on the tank by the liquid. However, if the oscillation frequency is near the resonant frequency, standing waves will not be formed but instead a large amplitude traveling wave or hydraulic jump occurs.

Figure 11 shows a typical tank geometry. If, say, the percentage volume of residual propellant remaining in the tank after venting during the flyback is $V_{RE}$, then the liquid depth h (Figure 11) is approximately

$$h \approx 1.7R_o\left[V_{RE}\left(1 + \frac{4R_o}{3L}\right)\right]^{2/3} \tag{1}$$

where it has been assumed that $(h/R_o)^2 \ll 1$.

In order to analyze the sloshing, we can replace the actual tank by an equivalent rectangular tank with length B:

$$B = L + 2\sqrt{2hR_o} \tag{2}$$

and width W:

$$W = 2\sqrt{2hR_o} \tag{3}$$

The equivalent flat-bottom liquid depth $h_o$ is

$$h_o = \pi R_o^2 V_{RE}\left(L + \frac{4}{3}R_o\right)/BW \tag{4}$$

(For a tank with $R_o$ = 10 ft, L = 20 ft, and $V_{RE}$ = 0.01 = 1%, these relations work out to be h = 1.1 ft, B = 20 + 9.4 = 29.4 ft, W = 9.4 ft, and $h_o$ = 0.38 ft.)

## Linearized Slosh Response

For the equivalent tank with small amounts of fluid, the fundamental slosh frequency is:

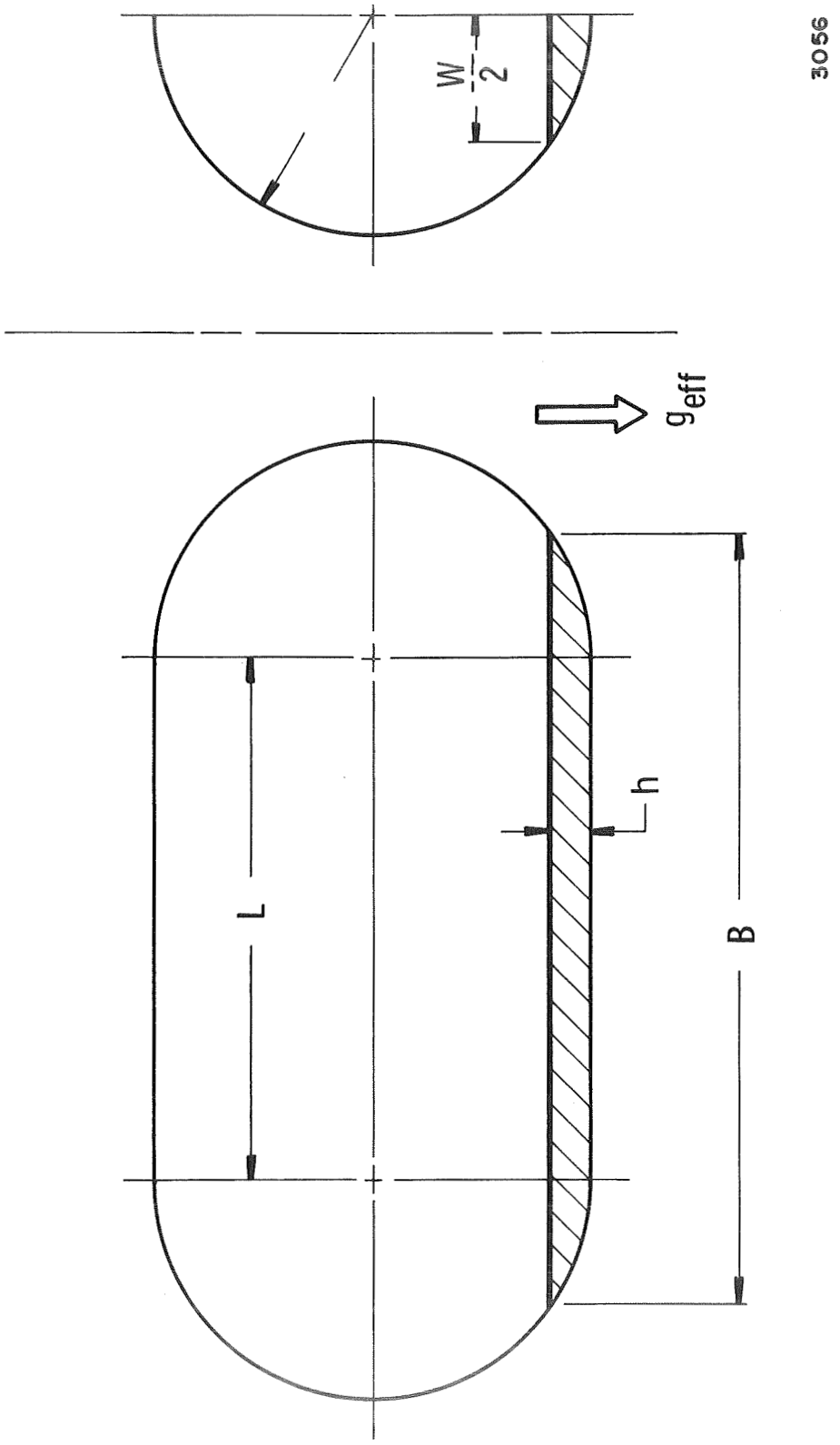


FIGURE 11.--TYPICAL TANK CONFIGURATION

$$\omega_1 = \pi(h_o g_{eff}/B^2)^{1/2} \tag{5}$$

since in the more general formula (ref. 3) the factor $\tanh(\pi h_o/B) \approx \pi h_o/B$.

The sloshing torques can be computed most easily by using the equivalent mechanical model shown in Figure 12. The slosh mass, $m_1$, is equal to

$$m_1 = \frac{8}{\pi^2}(\rho WBh_o) \approx 0.81\ \rho WBh_o \tag{6}$$

and is located at a depth below the free surface of $d_1 = -h_o$, that is, at the tank bottom. The rigid mass, $M_o$, is about equal to $\rho WBh_o - m_1 = 0.19\,\rho WBh_o$ and is located at a height above the free surface equal to $d_o = 0.5\,h_o(m_1/m_o) - 0.5\,h_o = 1.83\,h_o$. For small liquid depths, the total moment of inertia of the liquid about its center-of-mass (c.m.) is equal to the "frozen" moment of inertia; that is:

$$I_o + m_o(d_o + 0.5\,h_o)^2 + m_1(0.5\,h_o)^2 = \rho WBh_o\left(\frac{1}{12}\,h_o^2 + \frac{1}{16}\,B^2\right) \tag{7}$$

In order to calculate the disturbing moment caused by the tank oscillations, we will let the tank motion be given by a pitching rotation about the c.m. and a translation of the c.m. (The moment about any point can be calculated in terms of these two motions.) The total moment about the c.m., for an undamped pitching oscillation of $\theta_{cm}e^{i\omega t}$ is

$$M = \left(\frac{h_o}{B}\right)^2 M_s e^{i\omega t}\left\{0.985\left[\frac{\left(\frac{B}{h_o}\right)^2 + \pi^2\left(\frac{\omega}{\omega_1}\right)^2 + 0.25\,\pi^2\left(\frac{h_o^{\,2}}{B\omega_1^2}\right)^2}{1 - \left(\frac{\omega}{\omega_1}\right)^2}\right] + \pi^2\left(\frac{\omega}{\omega_1}\right)^2\left[\left(\frac{h_o}{B}\right)^2 + \frac{3}{4}\right]\right\} \tag{8}$$

where $M_s = \rho WB^3 g_{eff}\theta_{cm}/12$ is the static moment corresponding to a static tilt of the tank equal to the pitching amplitude $\theta_{cm}$. A similar equation can be written for the moment caused by the translation excitation, but Equation (8) is

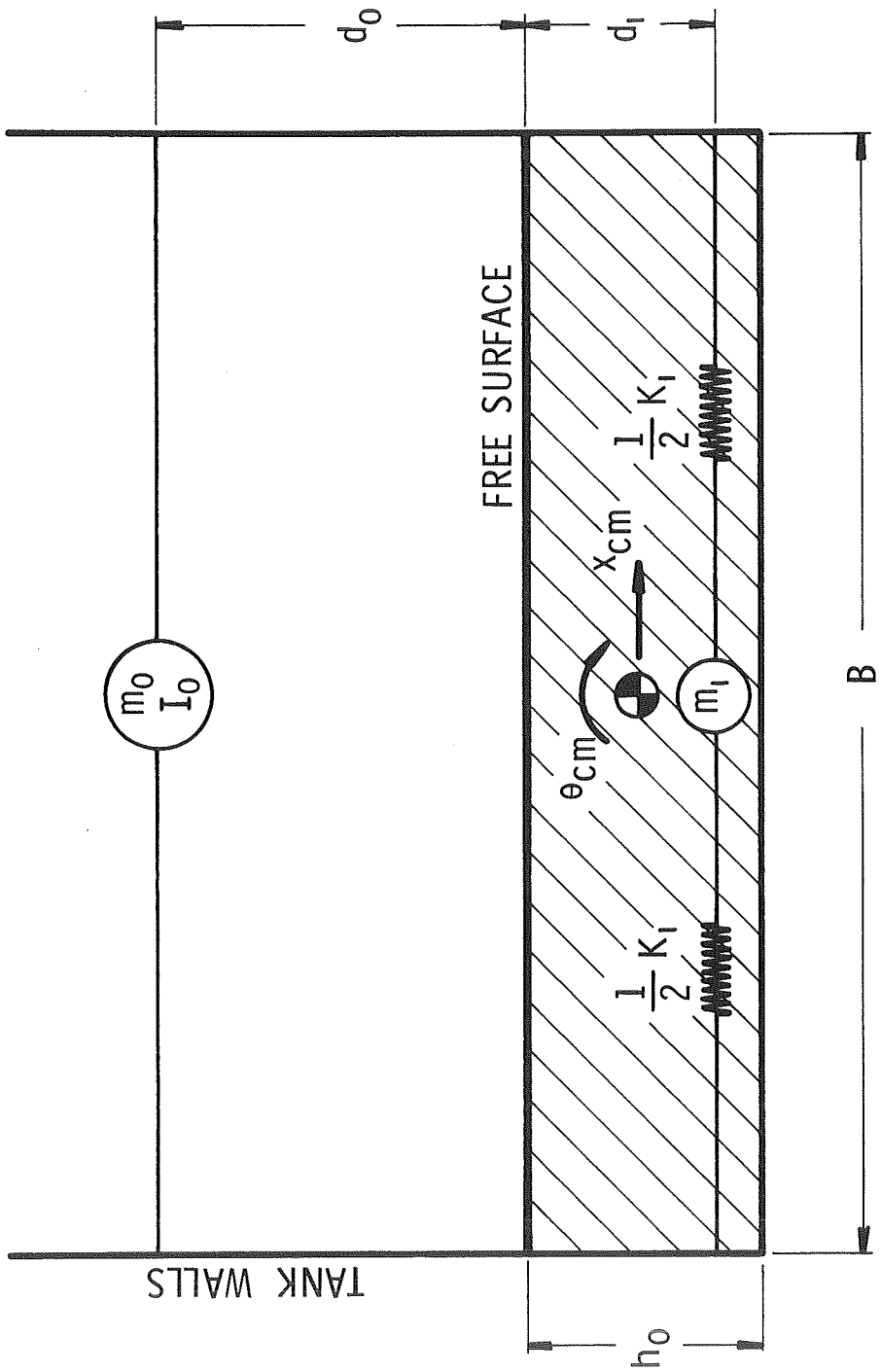


FIGURE 12.--EQUIVALENT MECHANICAL MODEL FOR LINEAR SLOSHING

sufficient to show the difference between the sloshing form of response and the traveling wave form. (The reason why $M \longrightarrow 0.985M_s$ instead of $M \longrightarrow M_s$ as $\omega^2 \longrightarrow 0$ is that only the fundamental slosh mass is included in the model, and higher order modes are neglected.)

A plot of $M/M_s$ versus $(\omega/\omega_1)^2$ is shown in Figure 13, for the particular tank geometry discussed previously (i.e., $h_o/B = 0.38/29.4 = 0.013$); the curve is almost independent of $h_o/B$ so long as $h_o/B \ll 1$. Right around resonance, Equation 8 is not valid, since, as we discussed previously, the traveling wave form of response predominates in this region. If the linear sloshing assumption was valid, the moment amplitude at resonance would depend on the viscous or baffle damping. (In other words, for an ideal fluid with no viscosity, the moment amplitude would be infinite.) Typical values of this "magnification" factor at resonance are about 10 to 15 in other forms of sloshing.

## Hydraulic Jump Response

In order to determine the actual magnitude of the liquid response near resonance, we will use the theory developed by Verhagen and Van Wijngaarden (ref. 2) for the fluid oscillations in long, shallow tanks. This "shallow water" theory, which is based on the ideal flow equations (no viscosity) but which does not assume potential flow, takes into account nonlinear, large amplitude motions. It predicts that a hydraulic jump occurs when the tank oscillations are near resonance, analogously to the shock wave that develops in a closed column of gas when the gas is oscillated at a resonant frequency.

The hydraulic jump travels at the shallow-water wave velocity $c_o = \sqrt{h_o g_{eff}}$, so the resonant frequency in the nonlinear approximation is still $\omega_1 = \pi(h_o g_{eff}/B^2)^{1/2}$. The amplitude of the resonant wave is not infinitely large, even for a zero-viscosity liquid, because there is energy dissipation at the wave front. Figure 14 shows a half-cycle of the motion.

Verhagen and Van Wijngaarden show that the hydraulic jump height is

$$\lambda = \frac{4}{\pi}\sqrt{\frac{2}{3}Bh_o\theta_{cm}} \approx 1.04\sqrt{Bh_o\theta_{cm}} \qquad (9)$$

for a pitching oscillation of the tank at the natural frequency. The same sort of jump occurs for a translation excitation.

The resonant moment exerted on the tank by the liquid is:

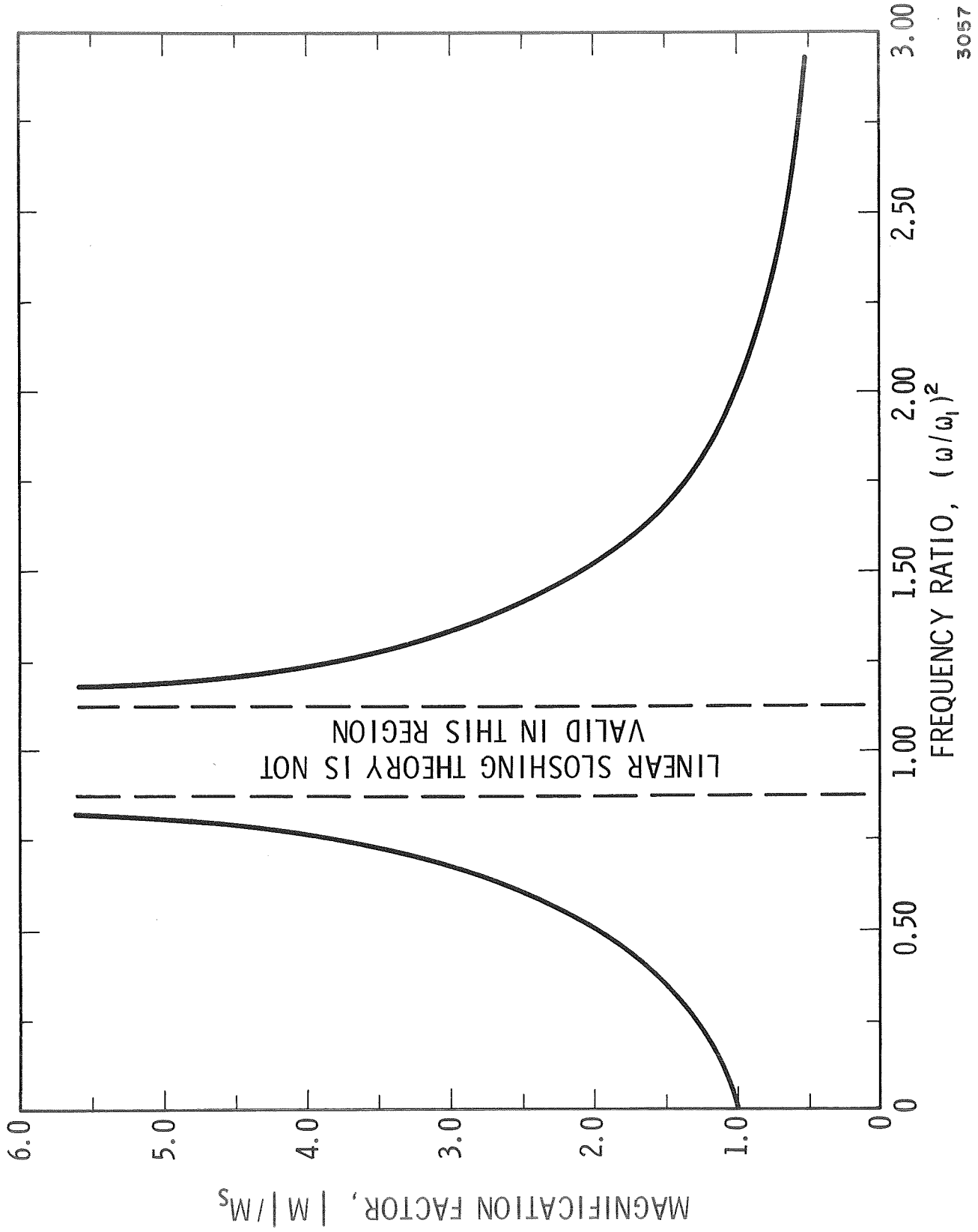


FIGURE 13.--MOMENT RESPONSE OF LINEAR SLOSH MODEL

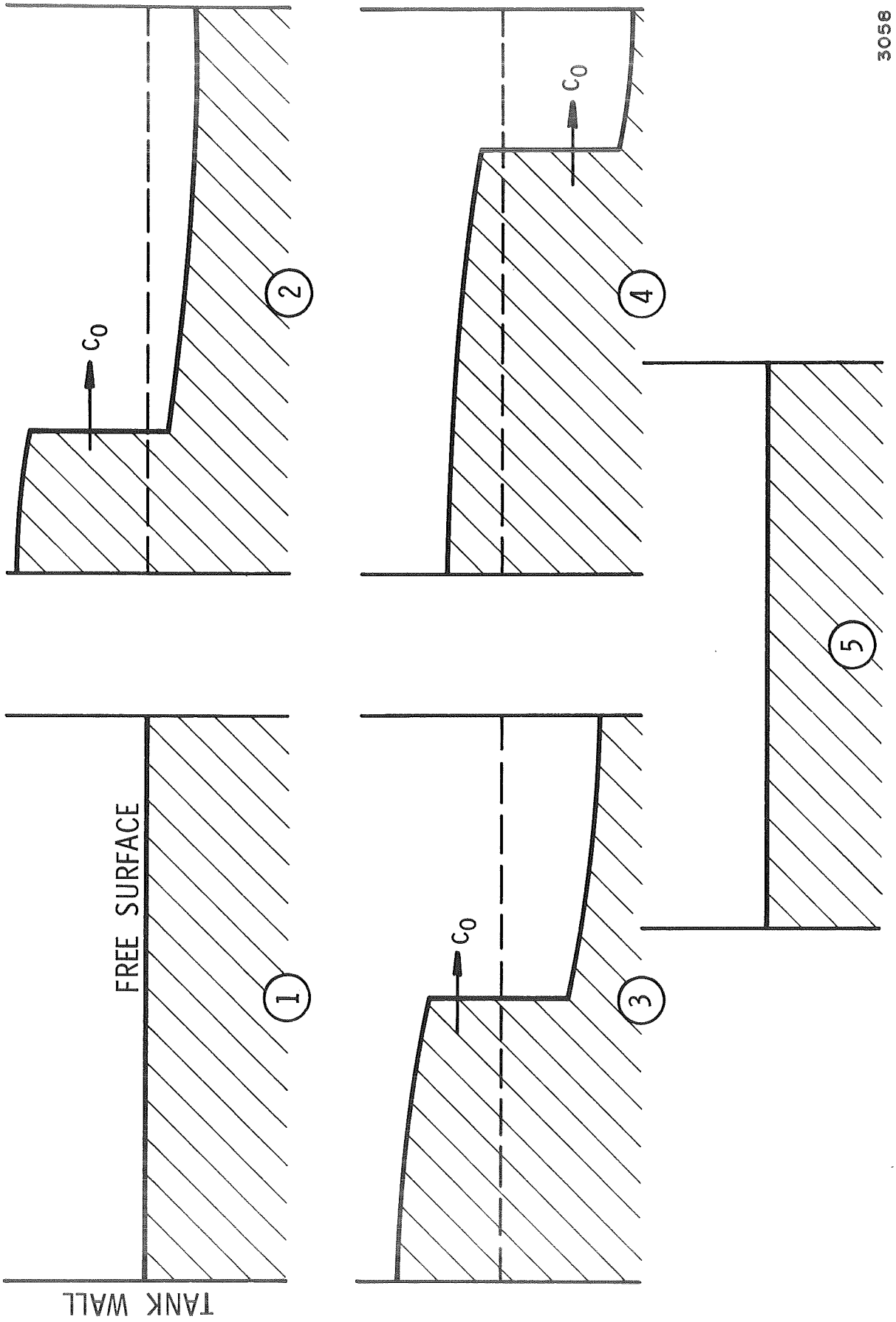


FIGURE 14.--ONE-HALF CYCLE OF HYDRAULIC JUMP RESPONSE

$$M = 2M_S\left(\frac{4}{\pi}\right)^4 e^{i\left(\omega t - \frac{\pi}{2}\right)}\sqrt{h_o/(B\theta_{cm})} \approx 5.25\, M_S e^{i\left(\omega t - \frac{\pi}{2}\right)}\sqrt{\frac{h_o}{B\theta_{cm}}} \quad (10)$$

For non-resonant excitation frequencies, the magnitude of the moment is related to the resonant moment by

$$\left|M\right| = \left|M_{\omega = \omega_1}\right| \left\{1 - \frac{B(\omega - \omega_1)^2}{32 g_{eff}\theta_{cm}}\right\} \quad (11)$$

The phase angle between the moment and the oscillation for the general case is given by

$$\psi = \frac{1}{2}\pi + 2 \arcsin\left[\frac{B(\omega - \omega_1)^2}{24 g_{eff}\theta_{cm}}\right]^{1/2} - \arcsin\left[\frac{B(\omega - \omega_1)^2}{96 g_{eff}\theta_{cm} - 3B(\omega - \omega_1)^2}\right] \quad (12)$$

As can be seen, the phase angle varies nonlinearly with both the excitation frequency and amplitude. More importantly, the relation between the dynamic moment and the static moment is now a function of the pitching amplitude, $\theta_{cm}$, and as $\theta_{cm} \longrightarrow 0$ the ratio $M/M_S \longrightarrow \infty$ (although, of course, both $M \longrightarrow 0$ and $M_S \longrightarrow 0$ as $\theta_{cm} \longrightarrow 0$).

A plot of the resonant moment response, Equation (10), is shown in Figure 15 for several values of $h_o/B$. The line labeled $\lambda = h_o$ corresponds to the conditions for which $h_o/B$ and $\theta_{cm}$ are such that the hydraulic jump height equals the equivalent liquid depth; this places an upper limit on $\theta_{cm}$ beyond which the theory is no longer valid. (The dashed line labeled $1/2\, B\theta_{cm} = h_o$ corresponds to the condition for which the static deflection of the liquid intersects the tank bottom.)

In order to appreciate the magnitudes of $M_S$ and M, let us consider the situation discussed previously: $R_o$ = 10 ft, L = 20 ft, and $V_{RE}$ = 1%. The volume of residual propellant is 105 cu ft, which corresponds to about 7900 lb of LOX or 465 lb of $LH_2$. The dimensions of the equivalent rectangular tank are B = 29.4 ft and W = 9.4 ft, and the equivalent liquid depth is $h_o$ = 0.38 ft, so $h_o/B$ = 0.013. If $g_{eff} = Ng_o$, where $g_o$ = 32.2 ft/sec$^2$, then the static moments work out to be

$$M_S = 1.5\, N\theta_{cm} \times 10^6 \text{ ft-lb for LOX}$$

$$M_S = 8.8\, N\theta_{cm} \times 10^4 \text{ ft-lb for LH2}$$

For $\theta_{cm} = 0.2°$, $|M| = 10\,M_s$ according to Equation 10* or Figure 15, so that the dynamic moment for this pitching amplitude is

$$M = 10\,M_s = 52,500 \text{ N ft-lb for LOX}$$

$$M = 10\,M_s = 3700 \text{ N ft-lb for LH2}$$

Thus, the moment is very large when the liquid oscillates in a long, shallow tank, even if the tank contains only a small mass of liquid. Another way to see this is to realize that for $\theta_{cm} = 0.2°$, the apparent shift in the cm of the liquid at resonance is 6.65 ft, according to the theory, and 0.665 ft for static conditions.

## Conclusions

It seems that dangerously large moments and shifts in the cm can occur whenever the vehicle is flying at a high angle-of-attack or during landing, even with small amounts of residual liquids. This is true even if it is not likely that the liquid will be excited into a resonant condition, simply because the dynamic forces created by a moving liquid amplify the already large static moment large for a long, shallow tank.

## References

1. Chu, W. H.; Dalzell, J. F.; and Modisette, J. E.: Theoretical and Experimental Study of Ship-Roll Stabilization Tanks. Journal of Ship Research. 12, Sept. 1968, pp. 165-180.

2. Verhagen, J. H. G.; and Van Wijngaarden, L.: Nonlinear Oscillations of Fluid in a Container. Journal of Fluid Mechanics. 22, part 4, pp. 737-751.

3. The Dynamic Behavior of Fluids in Moving Containers. Chapter 6, NASA SP-106, 1966.

*In all the equations, $\theta_{cm}$ must be expressed in radians, not degrees.

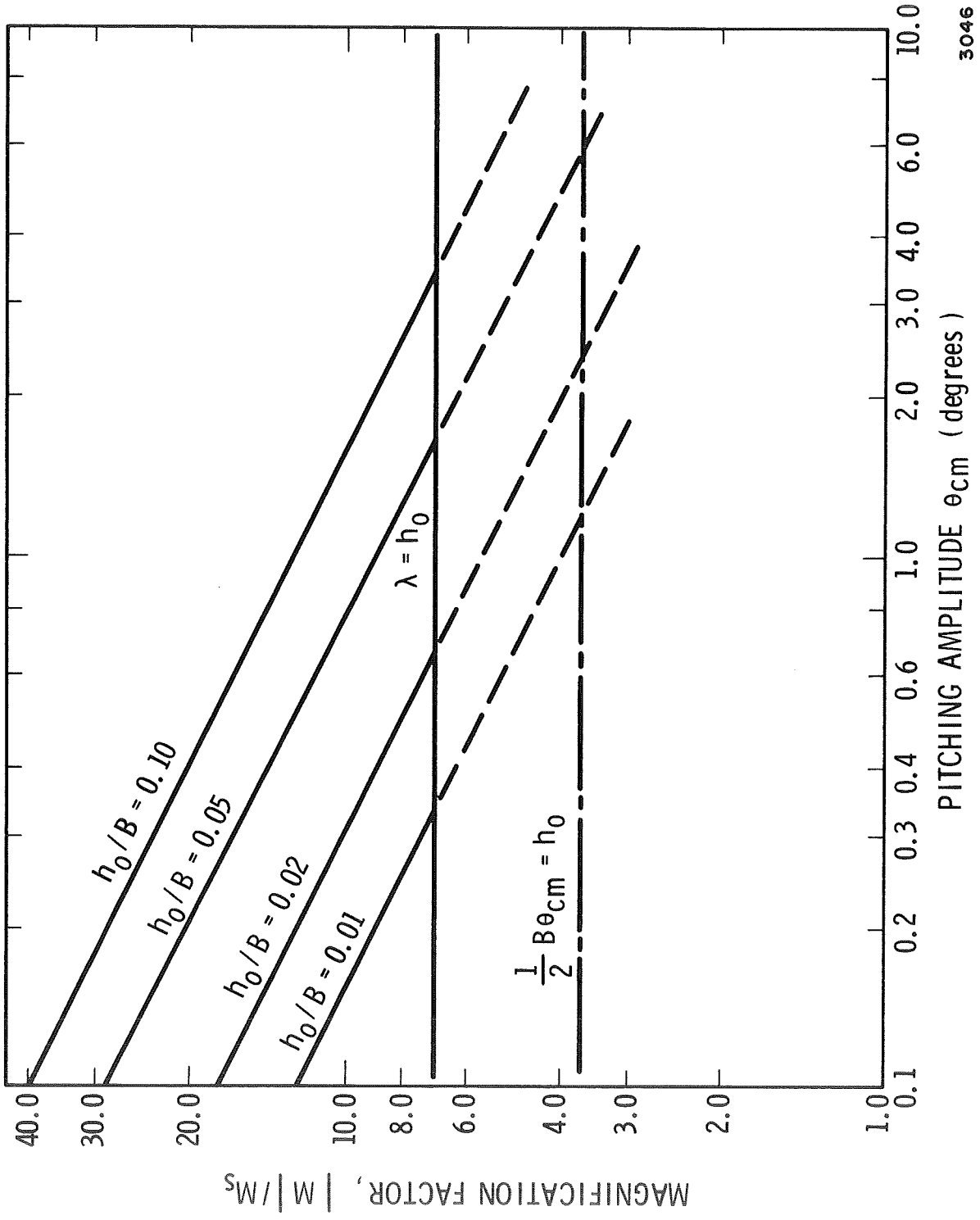


FIGURE 15.--MOMENT RESPONSE OF HYDRAULIC JUMP MODEL AT RESONANCE

# SLOSHING OF AN ARBITRARY TWO-DIMENSIONAL TANK WITH FLAT MEAN FREE SURFACE

## Introduction

During usual vertical rocket launching and acceleration in space, the gravity coincides with an axis of symmetry of the tank. The prediction of sloshing frequencies and a simplified mechanical model for such cases at arbitrary Bond number has been achieved in References 1, 2, and 3. However, for launching missiles and in particular for returning shuttle planes, effective gravity is not necessarily parallel to the axis of symmetry, if it exists. It is one of the objectives of the present project to give some estimate of the natural frequencies for fuel tanks at general orientation with respect to the direction of effective gravity $\underset{\sim}{g}$, presently for high-g only.

For an "accurate" prediction of the slosh frequencies, a three-dimensional analysis appears necessary. However, Budiansky's results (ref. 4) indicate that the natural frequencies for sloshing in a two-dimensional circle ("circular canal") are close to those of a sphere, of which the cross section in the meridian plane is a circle (Figure 16). This suggests that a good estimation of the effect of orientation on natural frequencies of sloshing may be obtained by a two-dimensional approximation to a three-dimensional tank. However, due to time limitations and present objectives, an ad hoc computer program is devised to yield desired results, with properly selected input data points specifying the tank shape and free surface. Some results are presented after description of the program.

## Mathematical Problem

For a two-dimensional tank, a set of rectangular coordinates may be used (Figure 17) with the origin at selected points on the free surface for convenience of specifying the shape of the contour and the direction of the normal, if needed.

The flow is assumed to be incompressible and irrotational. There exists a velocity potential $\phi$ satisfying

$$\nabla^2\phi = 0 \tag{13}$$

subject to the boundary condition that

$$\frac{\partial\phi}{\partial n} = 0 \qquad \text{on W (wall)} \tag{14}$$

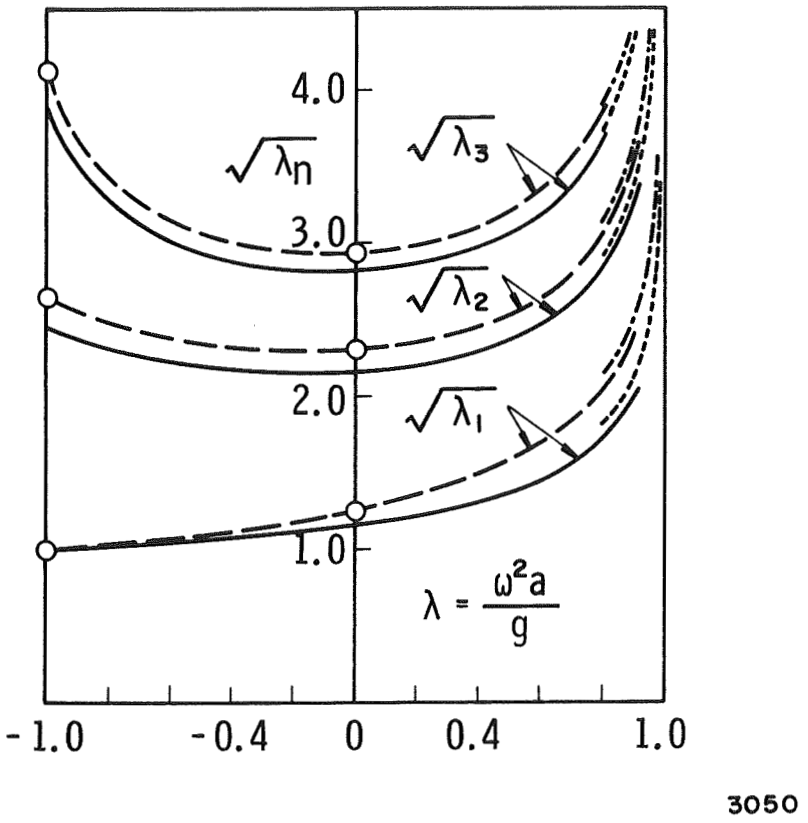


FIGURE 16. --FREQUENCIES FOR CIRCULAR CANAL (SOLID) AND SPHERICAL TANK (DASHED) (REF. 4)

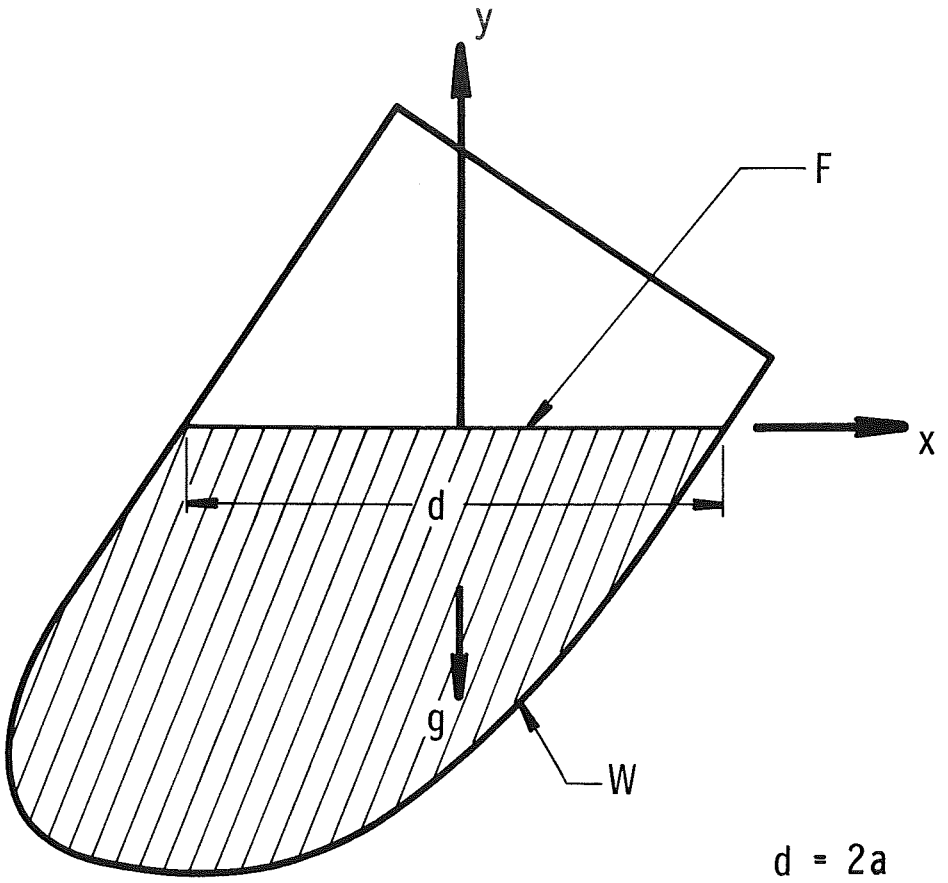


FIGURE 17. --COORDINATES FOR A TILTED TANK

$$\frac{\partial \phi}{\partial n} - \lambda \phi = 0 \qquad \text{on F (free surface)} \tag{15}$$

where

$$\lambda = \frac{\omega^2 a}{g} \tag{16}$$

n is outer normal.

The tank wall can be quite arbitrary; however, for simplicity of a "flexible" computer program, it will be assumed to be smooth and convex, which is the case in many applications. In some cases, with two sharp corners and even concave bottoms, the program to be presented may also be applicable if the length of the sides and that of the free surface and bottom are not too far different, respectively, and enough boundary points can be taken.

## Method of Solution

Numerical methods are considered due to their flexibility in application. In particular, for a general domain, it is convenient to use for the Laplace equation, either the Winslow method (refs. 1, 6) or the "machine transformation" (refs. 7, 8). The program to be presented is based on the machine transformation with modification of the computer program given in Reference 8. An inverse influence coefficient matrix is generated in the present program. Using this matrix, the natural frequencies are obtained through an eigenvalue subroutine. The orientation effect on the lowest frequency is sought.

## Influence Coefficient Method

For programming convenience, the vertical axis y is taken to be normal to the flat free surface at high-g. The shape of the two-dimensional tank is taken to be that in the plane of symmetry or some "approximate average location."

An attempt was made to modify the axisymmetric branch of the computer program of Reference 5, which employs "direct" influence coefficient calculations; i.e., the relaxation procedure was used to calculate the effect on the velocity potential on the free surface ($\phi_F$) due to a unit disturbance of the normal velocity $(\partial\phi/\partial n)_F$ at a node. However, $\phi_F = 0$ at the origin in non-axisymmetric flow ($m = 0$) but not in axisymmetric or two-dimensional flow. Consequently, in the present case, the direct influence coefficient method reduces to a Neumann problem in which the velocity potential is only defined within an

arbitrary constant and the equation matrix is singular. Thus, the relaxation method diverged even with constraint (say the average of $\phi$ over all nodes is $\overline{\phi} = 0$) adjusted at the end of every iteration. However, under-relaxation of the constraint at the right lower corner leads to converged direct influence coefficients, but not to the correct result for a two-dimensional rectangular tank. The difficulty lies in the fact that the constraint on $\phi$ may vary for each column of influence coefficient matrix and, further, it may differ for the same column for a different mode (eigenvector).

An inverse influence coefficient method was conceived; i.e., relaxation procedure was used to calculate the effect on $(\partial\phi/\partial n)_F$ due to a unit disturbance of the potential $\phi_F$ (which is proportional to a small oscillatory pressure). For some unknown reason, the modified low-g program failed to yield useful results. At first, it was thought that the method failed since not all influence coefficient solutions satisfy the boundary condition at the wall; further thought, however, led to the conclusion this is just another way of inverting a matrix using a much smaller storage location. It may also be comparable or cheaper in machine time-cost, if the ratio of surface points to volume points is less than some yet undetermined number. Since the corner flux in the Winslow method (ref. 6) may be either due to a wall motion or the free-surface motion, or both, Winslow's method is less certain than the "machine transformation" program employing well-known finite-difference rules. Hence, the latter was modified. It yielded good results for the test case of a rectangle of depth-width ratio, 2 (Table IV). There is a small first eigenvalue less than $10^{-3}$ or much smaller, depending on the relaxation factor or the convergence criterion. It corresponds to a rigid body mode ($\lambda = 0$) and therefore can be ignored.

TABLE IV. FREQUENCY PARAMETER

| Case/Mode No. | 1 | 2 | 3 |
|---|---|---|---|
| 11 × 6 mesh | 2.881 | 4.752 | 5.621 |
| 21 × 11 mesh | 3.049 | 5.676 | 7.728 |
| Exact | 3.1416 | 6.2832 | 9.4248 |

## Relaxation Procedure

The direct and reverse S.O.R. (successive over-relaxation) procedure in Reference 8 was used. However, in generating the inverse influence coefficients an optimum value of $\omega_R$, the over-relaxation factor, appears to exist but reduces to the neighborhood of unity when the angle of tilt is increased.

Furthermore, larger values of $\omega_R$ may lead to rapid divergence; hence, for simplicity, $\omega_R = 1$ is suggested for practical use and converges much faster than Winslow's optimization formula which is strictly valid for block tria-diagonal matrices with corresponding block relaxation procedures. However, a "trial-and-error" procedure to seek and use the optimum value may be incorporated in a refined program.

## Example

An example of a cylindrical shell with two hemi-ellipsoidal bulkheads was considered.*

Values of the first natural frequency parameter for a "half-full" and a "bottom-full" tank at several values of angle of tilt, $\theta$, are shown in Figure 18. The values relative to zero tilt are shown in Figure 19.

It is noted that variation in the third significant figure of the location of the free-surface point in some cases indicated a change of natural frequency in the fourth significant figure, while 10% error at a point near the corner can cause as much as about 30% error. Since the process of determining surface boundary points has not been computerized, it is subject to human error. Further, the mesh is relatively coarse; thus, some irregular points may still exist. For instance, the relative first natural frequency parameter for the half-full case at 40° tilt may be a little too high. Improvements, if needed, can be made in principle.

As an appropriate comparison of a circular cylindrical tank (ref. 9)† of large depth $[\lambda_1(\theta = 30°)/\lambda_1(\theta = 0°)] = 0.674$, while that of the half-full two-dimensional ellipsoidal bottom tank is 0.699; thus, the latter appears to yield a good estimate.

## Conclusions

An ad hoc computer program has been successfully completed for the calculation of the sloshing frequencies of a general, two-dimensional tank to show the effect of tilting on the first sloshing mode of a two-dimensional tank as an approximation to a tilted three-dimensional tank with a flat mean free surface. More calculations within ±90° tilt and comparison with experiments are needed to show the general usefulness of this or an improved program.

---

*This was suggested by Drs. F. T. Dodge and D. D. Kana.

†This paper was published after completion of the present work and is called to the writer's attention by Dr. F. T. Dodge.

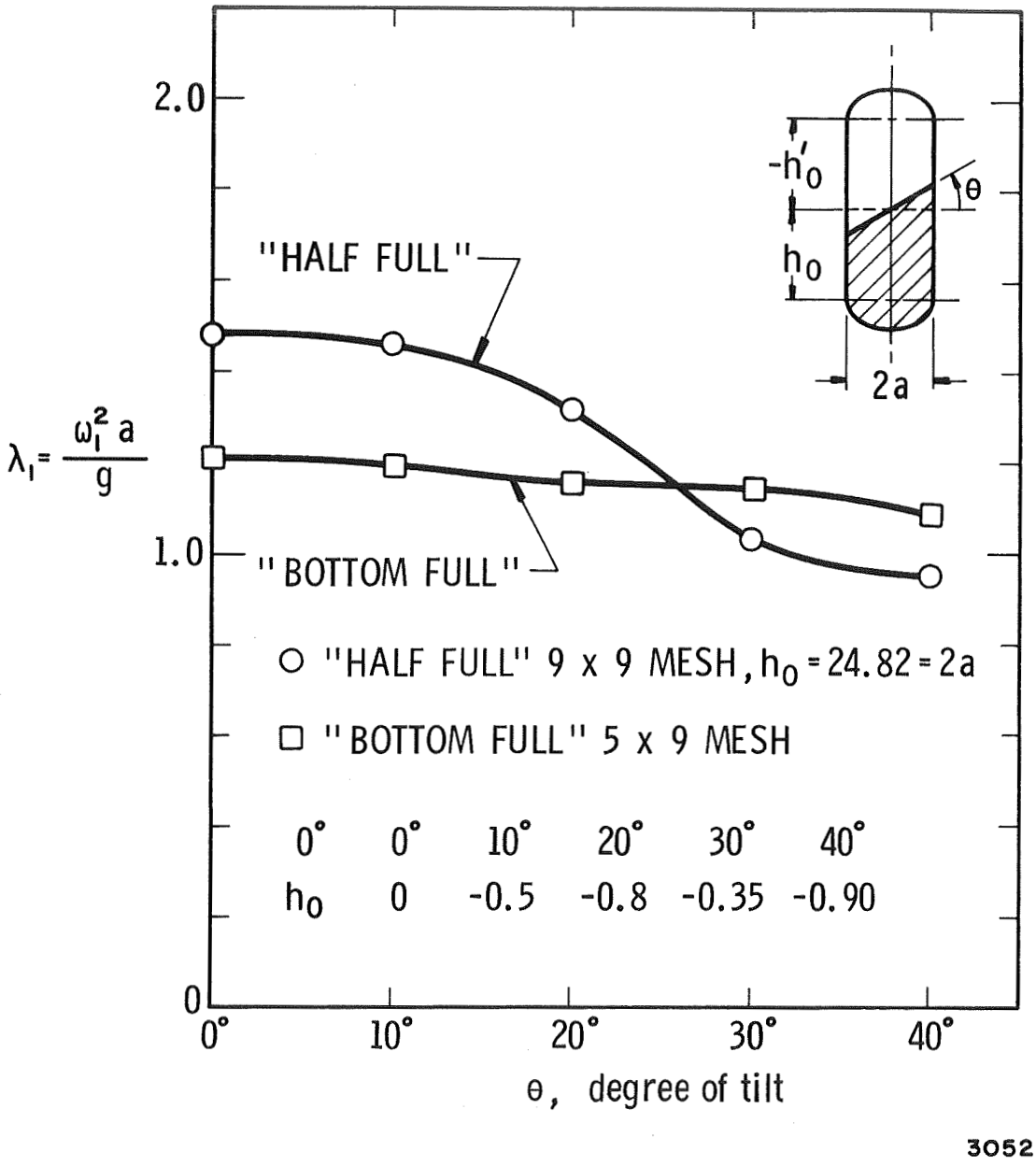


FIGURE 18. --VARIATION OF FIRST NATURAL FREQUENCY PARAMETER WITH ANGLE OF TWIST

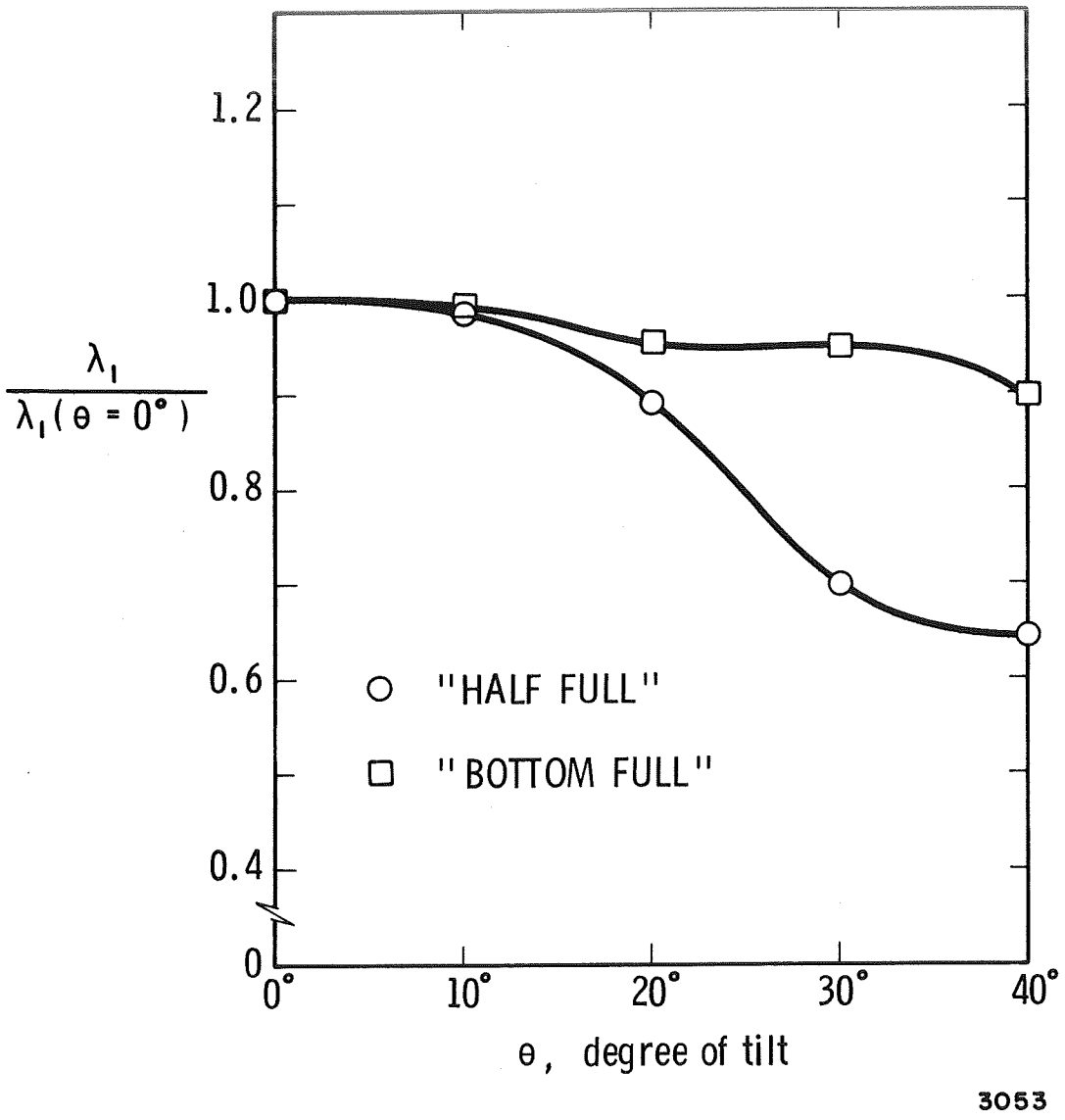


FIGURE 19.--VARIATION OF RELATIVE FREQUENCY PARAMETER WITH ANGLE OF TILT

The effect on other modes in a three-dimensional tank, say, transverse to the tilted plane, requires a three-dimensional program which can probably be achieved by the method of machine transformation. A practical matrix inversion may become preferable to the inverse influence coefficient method. It is expected that an order of magnitude larger machine time is required for good accuracy.

## References


1. Chu, Wen-Hwa. Low Gravity Fuel Sloshing in an Arbitrary Axisymmetric Rigid Tank. ASME Paper APM-EEE, 1970, to appear in J. Appl. Mech.

2. Concus, P.; Crane, G. F.; and Satterlee, H. M.: Low Gravity Lateral Sloshing in Hemispherically Bottomed Cylindrical Tanks. Proc. 1968 Heat Transfer & Fluid Mechanics Institute, Stanford Univ. Press, 1968, pp. 80-97.

3. Concus, P.; Crane, G. F.; and Satterlee, H. M.: Small Amplitude Lateral Sloshing in Spheroidal Containers Under Low Gravity Conditions. NASA CR-72500, LMSC-A944673, Lockheed Missiles and Space Co., Sunnyvale, California, February 4, 1969.

4. Budiansky, B: Sloshing of Liquids in Circular Canals and Spherical Tanks. J. Aerospace Sciences. 27, 3, March 1960.

5. Chu, W. H.; Gonzales, R.; Muller, A. F.; and Saathoff, D. R.: A Computer Program for Fuel Sloshing in an Axisymmetric Tank. Tech. Rept. No. 10, Contract No. NAS8-20290, SwRI Project 02-1846, August 1970.

6. Winslow, A. M.: Numerical Solutions of the Quasilinear Poisson Equations in a Non-uniform Triangular Mesh. J. Computational Physics. 1, 2, 1966, pp. 149-172.

7. Chu, W. H.: Development of a General Finite-Difference Approximation for a General Domain, Part I - Machine Transformation. Final Report, SwRI I.R. Project 02-9043, August 12, 1970.

8. Chu, W. H.: Development of a General Finite-Difference Approximation for a General Domain, Part II - A Numerical Method for Solving General MHD Duct Flow Problems. Final Report, SwRI I.R. Project 02-9043, Southwest Research Institute, August 26, 1970.

9. McNeill, W. A.; and Lamb, J. P.: Fundamental Sloshing Frequency for an Inclined, Fluid-Filled Right Circular Cylinder. J. Spacecraft. 7, 8, August 1970.

# APPENDIX

## A Computer Program for Sloshing in a General, Two-Dimensional Tank

By W. H. Chu

### Introduction

This is an ad hoc program to obtain the natural frequencies and mode shapes of a general, two-dimensional tank. A description of the basic principle has been given in the text. Since a simple parallelogram is used in the transformed plane, it is best suited for, but not strictly limited to, a smooth convex tank. A modified transformed domain may be required in some cases.

### Input SLOSH2D

1st card - (12A6) 72 columns of alphanumeric identification

2nd card - (415, 6E10.0) M, N, ITA, IRS, WA, WB, EPS, RLGTH, THETAD

| | | |
|---|---|---|
| M | = | number of points along each side |
| N | = | number of points along top or bottom |
| ITA | = | maximum number of iterations |
| IRS | = | restart number |
| WA | = | relaxation factor for linear approximations (mesh) |
| WB | = | initial relaxation factor for nonlinear solution (mesh and coefficients) |
| EPS | = | convergence factor for mesh |
| RLGTH | = | reference length (normalizing factor) |
| THETAD | = | counterclockwise tilt of flat free surface in degrees |

1st set of cards - (8E10.0) X(1,J), Y(1,J) J = 1,..., N
Coordinates for top boundary

2nd set of cards - (8E10.0) X(I,N), Y(I,N) I = 2,..., M-1
Coordinates for right boundary

3rd set of cards - (8E10.0) X(M,J), Y(M,J) J = 1,..., N
Coordinates for bottom boundary

4th set of cards - (8E10.0) X(I,1), Y(I,1) I = 2,..., M-1
Coordinates for left boundary

5th set of cards - (8E10.0) A, B, C, D, E, F (single card)*
Coefficients of general elliptic equation

6th set of cards - (8E10.0) ALPHA (I, J) I = 1, 3; J = 1, 4 (4 cards)
Three coefficients for boundary equation for each of four sides (J = 1, 2, 3, 4 are the top, right, bottom and left boundary in the transformed plane); all ALPHA (I, J) = 0 calculates coefficients (switch = 0).

## Directional Cosines

Directional cosine+ of the outer normal, $\alpha_1$ and $\alpha_2$ (I = 1, 2) with respect to x and y axis in the physical plane - - - program can be modified to calculate the average directional cosine of outer normal at each node by assuming each segment in the physical plane to be a straight line. At present, the program requires replacement of ALPHA (1, J), ALPHA (2, J) in the branch switch = 0 by appropriate analytic expressions through the use of subroutine ALFA see the tests if (Switch N.E. 0.) GO TO .... Only for quadrilateral contours one may use the input ALPHA (I, J), I = 1, 2 and ignore the replacement, while ALPHA (3, J) is always zero in the present problem. At corners in the transformed plane, directional cosines of both sides are needed. Otherwise, read all ALPHA (I, J) = 0, I = 1, 2, 3, J = 1, 2, 3, 4 to use the branch switch = 0.

## Output SLOSH2D

Most of the outputs are self-explanatory. The main outputs are the initial approximation to locations of the nodes in the physical plane, the final nonlinear approximation to these nodes, the influence coefficients†, and the eigenvalues, ($\omega_n^2 a/g$, n = 0, 1, 2, . . . ). (a = RLGTH) and eigenvectors.

## Other Remarks

See text.

## Listing

See following pages.

*For liquid sloshing A = C = 1, B = D = E = F = 0.
+ ALPHA (I, J), I = 1, 2.
†Its convergence or divergence indices are printed every 10 iterations.

```
      PROGRAM SLOSH2D(INPUT,OUTPUT,TAPE7,TAPE6,TAPE60=INPUT)

      DIMENSION X(40,24),Y(40,24),ITITLE(12)
      DIMENSION C(40,24,8),PHI(40,24),ALPHA(3,4),ALF4(40,4)
      DIMENSION PSI(40,24),FBARP(40,24),GBARP(40,24)
      DIMENSION CV(24),F(24,24),EVAL(24,24),EVEC(24,24),EVI(1,1)
      DIMENSION EIGVAL(24),NVAL(24)
      COMMON AE,BE,CE,DE,EE,SINT,COST,HO,X,Y
      KUN=6
      LUN=7
C     IF GENERATES INFLUENCE COEFF. IC,NE,0 ,1F NOT IC=0
C     IF INV.INF.COEFF.,VN=(F)PHI,IC=-1 OR  IC.LT.0
      IC=-1
      NDIM=24
      RHO=0.05
      BETAC=0.5
      WO=.01
   94 FORMAT (12A6)
   10 READ 94,ITITLE
      IF(EOF,60)20,30
   20 STOP
   30 READ 95,M,N,ITA,IRS,WA,WB,EPS,RLGTH,THETAD
   95 FORMAT (4I5,5E10.0)
      PRINT 96,ITITLE,M,N,ITA,WA,WB,EPS,IRS
   96 FORMAT (26H1TRIANGULAR MESH GENERATOR/,1X,12A6/,
     117H LOGICAL MESH IS ,I5,3H X ,I5/,32H MAXIMUM NUMBER OF ITERATIONS
     2 IS,I5/,40H RELAXATION FOR LINEAR APPROXIMATION IS ,F7.3/,
     353H INITIAL RELAXATION FACTOR FOR NONLINEAR SOLUTION IS ,F7.3/,
     428H EPSILON FOR CONVERGENCE IS ,E10.3/,19H RESTART IS NUMBER ,I5/)
      NM1=N-1
      MM1=M-1
      IF (IRS .EQ. 0) GO TO 3003
      GO TO (3001,1061,3006),IRS
 3003 CONTINUE
      READ 200,(X(1,J),Y(1,J),J=1,N)
      READ 200,(X(I,N),Y(I,N),I=2,MM1)
      READ 200,(X(M,J),Y(M,J),J=1,N)
      READ 200,(X(I,1),Y(I,1),I=2,MM1)
  200 FORMAT (8E10.0)
      DO 93 J=1,N
      X(1,J)=X(1,J)/RLGTH
      Y(1,J)=Y(1,J)/RLGTH
      X(M,J)=X(M,J)/RLGTH
   93 Y(M,J)=Y(M,J)/RLGTH
      DO 92 I=2,MM1
      X(I,N)=X(I,N)/RLGTH
      Y(I,N)=Y(I,N)/RLGTH
      X(I,1)=X(I,1)/RLGTH
   92 Y(I,1)=Y(I,1)/RLGTH
C     INTERPOLATE FROM BOUNDARIES TO GET FIRST GUESS
      DO 100 J=2,NM1
      DO 100 I=2,MM1
      X(I,J)=X(I,J-1)+X(I-1,J)-X(I-1,J-1)
      Y(I,J)=Y(I,J-1)+Y(I-1,J)-Y(I-1,J-1)
  100 CONTINUE
```

```
      GO TO 3002
C     RESTART 1
 3001 READ (LUN) ((X(I,J),Y(I,J),I=1,M),J=1,N)
      WRITE(KUN) ((X(I,J),Y(I,J),I=1,M),J=1,N)
 3002 CONTINUE
      YTEMP=((Y(1,1)-Y(M,1))/M)**2
      XTEMP=((X(1,N)-X(1,1))/N)**2
      DO 97 J=2,NM1
      DO 97 I=2,MM1
      C(I,J,1)=YTEMP
      C(I,J,2)=0.0
      C(I,J,3)=XTEMP
   97 CONTINUE
      IDIR=-1
C*****TIMING INFO
      CALL SECOND(TIM)
      PRINT 5000,TIM
 5000 FORMAT(*0TIME  *,E16.7/)
      DO 103 MOST=1,ITA
      SX=0.0
      KIT=MOST
      SY=0.0
      SRX=0.0
      SRY=0.0
      IDIR=-IDIR
      DO 102 K=2,MM1
      DO 102 L=2,NM1
      IF(IDIR) 1001,1002,1002
 1001 I=MM1-K+2
      J=NM1-L+2
      GO TO 1003
 1002 I=K
      J=L
 1003 CONTINUE
      XTEMP=(X(I-1,J-1)+X(I+1,J+1)+X(I,J-1)+X(I,J+1)+X(I-1,J)+X(I+1,J)
     1 )/6.0
      YTEMP=(Y(I-1,J-1)+Y(I+1,J+1)+Y(I,J-1)+Y(I,J+1)+Y(I-1,J)+Y(I+1,J)
     1 )/6.0
      RX=(X(I,J)-XTEMP)*WA
      RY=(Y(I,J)-YTEMP)*WA
      X(I,J)=X(I,J)-RX
      Y(I,J)=Y(I,J)-RY
      SX=SX+X(I,J)**2
      SY=SY+Y(I,J)**2
      SRX=SRX+RX**2
      SRY=SRY+RY**2
  102 CONTINUE
      IF (MOST-20*(MOST/20)) 1022,1021,1022
 1021 WRITE (KUN) ((X(I,J),Y(I,J),I=1,M),J=1,N)
      REWIND KUN
      IRS=1
      IF(MOST .EQ. 20) PRINT 410,IRS
  410 FORMAT(21HOYOU MAY USE RESTART ,I4)
 1022 CONTINUE
      SRX=SQRT(SRX/SX)
      SRY=SQRT(SRY/SY)
      IF (SRX .LE. EPS .AND. SRY .LE. EPS) 105,103
  103 CONTINUE
```

```
      PRINT 201,SRX,SRY
  201 FORMAT(51H1PROCESS DID NOT CONVERGE FOR INITIAL APPROXIMATION/,
     110H EPS=X IS ,E15.7,12H   EPS=Y IS ,E15.7//,41H X AND Y VALUES ARE
     2 PRINTED BELOW BY ROWS/)
      DO 104 I=1,M
  104 PRINT 202,(X(I,J),Y(I,J),J=1,N)
  202 FORMAT (8E15.7)
      WRITE (KUN) ((X(I,J),Y(I,J),I=1,M),J=1,N)
      REWIND KUN
      IRS=1
      PRINT 410,IRS
      STOP
  105 PRINT 203,KIT
  203 FORMAT (58H1PROCESS CONVERGED FOR INITIAL APPROXIMATION ON ITERATI
     1ON ,I5/,33H X AND Y ARE PRINTED BELOW BY ROW/)
C*****TIMING INFO
      CALL SECOND(TIM)
      PRINT 5000,TIM
      DO 106 I=1,M
      PRINT 202,(X(I,J),Y(I,J),J=1,N)
  106 CONTINUE
      WRITE (KUN) ((X(I,J),Y(I,J),I=1,M),J=1,N)
     1 ,(((C(I,J,K),I=1,M),J=1,N),K=1,3)
      REWIND KUN
      IRS=2
      PRINT 410,IRS
      GO TO 1062
C     RESTART 2
 1061 READ (LUN) ((X(I,J),Y(I,J),I=1,M),J=1,N)
     1 ,(((C(I,J,K),I=1,M),J=1,N),K=1,3)
      WRITE(KUN) ((X(I,J),Y(I,J),I=1,M),J=1,N)
     1 ,(((C(I,J,K),I=1,M),J=1,N),K=1,3)
 1062 CONTINUE
      WX=WB
      WY=WB
      IDIR=-1
C*****TIMING INFO
      CALL SECOND(TIM)
      PRINT 5000,TIM
      DO 135 MOST=1,ITA
      IDIR=-IDIR
      KIT=MOST
      SRX=0.0
      SRY=0.0
      SX=0.0
      SY=0.0
      DO 110 I=2,MM1
      DO 110 J=2,NM1
      DXDX=((X(I-1,J-1)+2.0*X(I-1,J)+X(I,J+1))-(X(I,J-1)+2.0*X(I+1,J)
     1 +X(I+1,J+1)))/6.0
      DYDX=((Y(I-1,J-1)+2.0*Y(I-1,J)+Y(I,J+1))-(Y(I,J-1)+2.0*Y(I+1,J)
     1 +Y(I+1,J+1)))/6.0
      GAMMA=DXDX**2+DYDX**2
      DXDY=((X(I-1,J)+2.0*X(I,J+1)+X(I+1,J+1))-(X(I-1,J-1)+2.0*X(I,J-1)
     1 +X(I+1,J)))/6.0
      DYDY=((Y(I-1,J)+2.0*Y(I,J+1)+Y(I+1,J+1))-(Y(I-1,J-1)+2.0*Y(I,J-1)
     1 +Y(I+1,J)))/6.0
      ALPHA=DXDY**2+DYDY**2
```

```
      BETA=DXDY*DXDX*DYDX*DYDY
      CP1=ALPHA*BETA
      CP2=BETA
      CP3=GAMMA*BETA
      CP1=BETAC*CP1+(1.0-BETAC)*C(I,J,1)
      CP2=BETAC*CP2+(1.0-BETAC)*C(I,J,2)
      CP3=BETAC*CP3+(1.0-BETAC)*C(I,J,3)
      C(I,J,1)=CP1
      C(I,J,2)=CP2
      C(I,J,3)=CP3
  110 CONTINUE
      DO 120 K=2,MM1
      DO 120 L=2,NM1
      IF(IDIR) 1011,1012,1012
 1011 I=MM1-K+2
      J=NM1-L+2
      GO TO 1013
 1012 I=K
      J=L
 1013 CONTINUE
      C1=C(I,J,1)
      C2=C(I,J,2)
      C3=C(I,J,3)
      C4=C1
      C5=C2
      C6=C3
      SUMC=C1+C2+C3+C4+C5+C6
      IF (ABS(SUMC) - 1.0E-10) 120,120,111
  111 XTEMP=(C1*X(I-1,J)+C2*X(I-1,J-1)+C3*X(I,J-1)+C4*X(I+1,J)
     1 +C5*X(I+1,J+1)+C6*X(I,J+1))/SUMC
      YTEMP=(C1*Y(I-1,J)+C2*Y(I-1,J-1)+C3*Y(I,J-1)+C4*Y(I+1,J)
     1 +C5*Y(I+1,J+1)+C6*Y(I,J+1))/SUMC
      RX=(X(I,J)-XTEMP)*WX
      RY=(Y(I,J)-YTEMP)*WY
      X(I,J)=X(I,J)-RX
      Y(I,J)=Y(I,J)-RY
      SRX=SRX+RX**2
      SRY=SRY+RY**2
      SX=SX+X(I,J)**2
      SY=SY+Y(I,J)**2
  120 CONTINUE
      IF (MOST-20*(MOST/20)) 3005,3004,3005
 3004 WRITE (KUN) ((X(I,J),Y(I,J),I=1,M),J=1,N)
     1 ,(((C(I,J,K),I=1,M),J=1,N),K=1,3)
      REWIND KUN
      IRS=2
      IF(MOST .EQ. 20) PRINT 410,IRS
 3005 CONTINUE
      IF (KIT-1) 126,126,127
  126 SPRX=SRX
      SPRY=SRY
  127 EPSCX=SQRT(SRX/SX)
      EPSCY=SQRT(SRY/SY)
      IF (EPSCX .LE. EPS .AND. EPSCY .LE. EPS) GO TO 140
      ETAX=SQRT(SRX/SPRX)
      ETAY=SQRT(SRY/SPRY)
      ELX=(WX*ETAX-1.0)/(WX*SQRT(ETAX))
      ELY=(WY*ETAY-1.0)/(WY*SQRT(ETAY))
```

```
      IF (ABS(ELX)-1.0) 129,129,128
  128 WAX=WX
      GO TO 130
  129 WAX=2.0/(1.0+SQRT(1.0-ELX**2))-WO
  130 IF (ABS(ELY)-1.0) 132,132,131
  131 WAY=WY
      GO TO 133
  132 WAY=2.0/(1.0+SQRT(1.0-ELY**2))-WO
  133 WX=RHO*WAX+(1.0-RHO)*WX
      WY=RHO*WAY+(1.0-RHO)*WY
      SPRX=SRX
      SPRY=SRY
  135 CONTINUE
      PRINT 204,KIT,EPSCX,EPSCY
  204 FORMAT (43H1NONLINEAR SOLUTION DID NOT CONVERGE AFTER ,I5,11H ITER
     1ATIONS/,10H EPS-X IS ,E15.7,12H   EPS-Y IS ,E15.7/,34H X AND Y ARE
     2 PRINTED BELOW BY ROWS/)
      DO 136 I=1,M
      PRINT 202,(X(I,J),Y(I,J),J=1,N)
  136 CONTINUE
      WRITE (KUN) ((X(I,J),Y(I,J),I=1,M),J=1,N)
     1 ,(((C(I,J,K),I=1,M),J=1,N),K=1,3)
      IRS=2
      PRINT 410,IRS
      STOP
  140 PRINT 205,KIT
  205 FORMAT (42H1NONLINEAR SOLUTION CONVERGED ON ITERATION,I5/,
     134H X AND Y ARE PRINTED BELOW BY ROWS/)
C*****TIMING INFO
      CALL SECOND(TIM)
      PRINT 5000,TIM
      DO 141 I=1,M
      PRINT 202,(X(I,J),Y(I,J),J=1,N)
  141 CONTINUE
      WRITE (KUN) ((X(I,J),Y(I,J),I=1,M),J=1,N)
     1 ,(((C(I,J,K),I=1,M),J=1,N),K=1,3)
      IRS=3
      PRINT 410,IRS
      GO TO 3007
C     RESTART 3
 3006 READ (LUN) ((X(I,J),Y(I,J),I=1,M),J=1,N)
     1 ,(((C(I,J,K),I=1,M),J=1,N),K=1,3)
      WRITE(KUN) ((X(I,J),Y(I,J),I=1,M),J=1,N)
     1 ,(((C(I,J,K),I=1,M),J=1,N),K=1,3)
 3007 CONTINUE
      READ 200,CAPA,CAPB,CAPC,CAPD,CAPE,CAPF
      PRINT 1160
      SWITCH=0.0
      DO 500 J=1,4
      READ 200,(ALPHA(I,J),I=1,3)
      PRINT 1100,(ALPHA(I,J),I=1,3)
      SWITCH=SWITCH+ABS(ALPHA(1,J))+ABS(ALPHA(2,J))+ABS(ALPHA(3,J))
  500 CONTINUE
      PI=3.14159265
      EPS=1.0E-5
      RHO=0.025
      THETA=THETAD*PI/180.
      BT=-1.0
```

```
      HO=-.08
      HO=HO/RLGTH
      A=12.42
      A=A/RLGTH
      B=A/SQRT(2.0)
      A2=A**2
      B2=B**2
      SINT=SIN(THETA)
      COST=COS(THETA)
      AE=COST**2/A2+SINT**2/B2
      BE=COST*SINT*(2.0/B2-2.0/A2)
      CE=SINT**2/A2+COST**2/B2
      DE=2.0*HO*SINT/B2
      EE=2.0*HO*COST/B2
C*****TIMING INFO
      CALL SECOND(TIM)
      PRINT 5000,TIM
      DO 505 I=1,M
      DO 505 J=1,N
      FBARP(I,J)=0.0
  505 CONTINUE
C     INTERIOR POINTS
      DO 510 I=2,MM1
      DO 510 J=2,NM1
      XXI=((X(I-1,J)+2.0*X(I,J+1)+X(I+1,J+1))-(X(I-1,J-1)+2.0*X(I,J-1)
     1    +X(I+1,J)))/6.0
      YXI=((Y(I-1,J)+2.0*Y(I,J+1)+Y(I+1,J+1))-(Y(I-1,J-1)+2.0*Y(I,J-1)
     1    +Y(I+1,J)))/6.0
      XETA=((X(I-1,J-1)+2.0*X(I-1,J)+X(I,J+1))-(X(I,J-1)+2.0*X(I+1,J)
     1     +X(I+1,J+1)))/6.0
      YETA=((Y(I-1,J-1)+2.0*Y(I-1,J)+Y(I,J+1))-(Y(I,J-1)+2.0*Y(I+1,J)
     1     +Y(I+1,J+1)))/6.0
      X2XI=X(I,J+1)-2.0*X(I,J)+X(I,J-1)
      Y2XI=Y(I,J+1)-2.0*Y(I,J)+Y(I,J-1)
      XXIETA=((X(I-1,J)+X(I,J+1)+X(I,J-1)+X(I+1,J))-(X(I-1,J-1)
     1       +X(I+1,J+1)+2.0*X(I,J)))*.5
      YXIETA=((Y(I-1,J)+Y(I,J+1)+Y(I,J-1)+Y(I+1,J))-(Y(I-1,J-1)
     1       +Y(I+1,J+1)+2.0*Y(I,J)))*.5
      X2ETA=X(I-1,J)-2.0*X(I,J)+X(I+1,J)
      Y2ETA=Y(I-1,J)-2.0*Y(I,J)+Y(I+1,J)
      CJ=XXI*YETA-XETA*YXI
      XIX=YETA/CJ
      XIY=-XETA/CJ
      ETAX=-YXI/CJ
      ETAY=XXI/CJ
      CJXI=YETA*X2XI+XXI*YXIETA-YXI*XXIETA-XETA*Y2XI
      CJETA=YETA*XXIETA+XXI*Y2ETA-YXI*X2ETA-XETA*YXIETA
      XIXX=(XIX*YXIETA+ETAX*Y2ETA)/CJ-YETA*(XIX*CJXI+ETAX*CJETA)/CJ**2
      XIXY=(XIY*YXIETA+ETAY*Y2ETA)/CJ-YETA*(XIY*CJXI+ETAY*CJETA)/CJ**2
      ETAXX=-(XIX*Y2XI+ETAX*YXIETA)/CJ+YXI*(XIX*CJXI+ETAX*CJETA)/CJ**2
      ETAXY=-(XIY*Y2XI+ETAY*YXIETA)/CJ+YXI*(XIY*CJXI+ETAY*CJETA)/CJ**2
      ABAR=CAPA*XIX**2+CAPB*XIY*XIX+CAPC*XIY**2
      BBAR=2.*CAPA*XIX*ETAX+CAPB*(XIY*ETAX+ETAY*XIX)+2.*CAPC*XIY*ETAY
      CBAR=CAPA*ETAX**2+CAPB*ETAX*ETAY+CAPC*ETAY**2
      DBAR=CAPA*XIXX+CAPB*XIXY-CAPC*XIXX+CAPD*XIX+CAPE*XIY
      EBAR=CAPA*ETAXX+CAPB*ETAXY-CAPC*ETAXX+CAPD*ETAX+CAPE*ETAY
      FBAR=CAPF
      C(I,J,1)=.5*BBAR+CBAR+DBAR/6.+EBAR/3.
```

```
      C(I,J,2)=-.5*BBAR-DBAR/6.+EBAR/6.
      C(I,J,3)=ABAR+.5*BBAR-DBAR/3.-EBAR/6.
      C(I,J,4)=.5*BBAR+CBAR-DBAR/6.-EBAR/3.
      C(I,J,5)=-.5*BBAR+DBAR/6.-EBAR/6.
      C(I,J,6)=ABAR+.5*BBAR+DBAR/3.+EBAR/6.
      C(I,J,7)=0.0
      C(I,J,8)=2.*ABAR+BBAR+2.*CBAR
  510 CONTINUE
C     RIGHT BOUNDARY
      J=N
      DO 530 I=2,MM1
      XXI=.5*(3.*X(I,J)-4.*X(I,J-1)+X(I,J-2))
      YXI=.5*(3.*Y(I,J)-4.*Y(I,J-1)+Y(I,J-2))
      XETA=.5*(X(I-1,J)-X(I+1,J))
      YETA=.5*(Y(I-1,J)-Y(I+1,J))
      CJ=XXI*YETA-XETA*YXI
      IF(SWITCH.NE.0) GO TO 525
      CALL ALFA(I,J,2,BT,ALPHA)
  525 CONTINUE
      ALF1=(ALPHA(1,2)*YETA-ALPHA(2,2)*XETA)/CJ
      ALF2=(-ALPHA(1,2)*YXI+ALPHA(2,2)*XXI)/CJ
      ALF3=ALPHA(3,2)
      ALF4(I,2)=0.0
      C(I,J,1)=-.5*ALF2
      C(I,J,2)=0.0
      C(I,J,3)=2.*ALF1
      C(I,J,4)=.5*ALF2
      C(I,J,5)=0.0
      C(I,J,6)=0.0
      C(I,J,7)=-.5*ALF1
      C(I,J,8)=1.5*ALF1+ALF3
  530 CONTINUE
C     LOWER BOUNDARY
      I=M
      DO 540 J=2,NM1
      XXI=.5*(X(I,J+1)-X(I,J-1))
      YXI=.5*(Y(I,J+1)-Y(I,J-1))
      XETA=-.5*(3.*X(I,J)-4.*X(I-1,J)+X(I-2,J))
      YETA=-.5*(3.*Y(I,J)-4.*Y(I-1,J)+Y(I-2,J))
      CJ=XXI*YETA-XETA*YXI
      IF(SWITCH.NE.0) GO TO 535
      CALL ALFA(I,J,3,BT,ALPHA)
  535 CONTINUE
      ALF1=(ALPHA(1,3)*YETA-ALPHA(2,3)*XETA)/CJ
      ALF2=(-ALPHA(1,3)*YXI+ALPHA(2,3)*XXI)/CJ
      ALF3=ALPHA(3,3)
      ALF4(J,3)=0.0
      C(I,J,1)=-2.*ALF2
      C(I,J,2)=0.0
      C(I,J,3)=.5*ALF1
      C(I,J,4)=0.0
      C(I,J,5)=0.0
      C(I,J,6)=-.5*ALF1
      C(I,J,7)=.5*ALF2
      C(I,J,8)=-1.5*ALF2+ALF3
  540 CONTINUE
C     LEFT BOUNDARY
      J=1
```

```
      DO 550 I=2,MM1
      XXI=-.5*(3.*X(I,J)-4.*X(I,J+1)+X(I,J+2))
      YXI=-.5*(3.*Y(I,J)-4.*Y(I,J+1)+Y(I,J+2))
      XETA=.5*(X(I-1,J)-X(I+1,J))
      YETA=.5*(Y(I-1,J)-Y(I+1,J))
      CJ=XXI*YETA-XETA*YXI
      IF(SWITCH.NE.0) GO TO 545
      CALL ALFA(I,J,4,BT,ALPHA)
  545 CONTINUE
      ALF1=(ALPHA(1,4)*YETA-ALPHA(2,4)*XETA)/CJ
      ALF2=(-ALPHA(1,4)*YXI+ALPHA(2,4)*XXI)/CJ
      ALF3=ALPHA(3,4)
      ALF4(I,4)=0.0
      C(I,J,1)=-.5*ALF2
      C(I,J,2)=0.0
      C(I,J,3)=0.0
      C(I,J,4)=.5*ALF2
      C(I,J,5)=0.0
      C(I,J,6)=-2.*ALF1
      C(I,J,7)=.5*ALF1
      C(I,J,8)=-1.5*ALF1*ALF3
  550 CONTINUE
C     LOWER RIGHT CORNER
      XXI=.5*(3.*X(M,N)-4.*X(M,N-1)+X(M,N-2))
      YXI=.5*(3.*Y(M,N)-4.*Y(M,N-1)+Y(M,N-2))
      XETA=-.5*(3.*X(M,N)-4.*X(M-1,N)+X(M-2,N))
      YETA=-.5*(3.*Y(M,N)-4.*Y(M-1,N)+Y(M-2,N))
      CJ=XXI*YETA-XETA*YXI
      IF(SWITCH.NE.0) GO TO 580
      CALL ALFA(M,N,2,BT,ALPHA)
      CALL ALFA(M,N,3,BT,ALPHA)
  580 CONTINUE
      ALF1=YETA*(ALPHA(1,2)+ALPHA(1,3))/CJ-XETA*(ALPHA(2,2)+ALPHA(2,3))
     1     /CJ
      ALF2=-YXI*(ALPHA(1,2)+ALPHA(1,3))/CJ+XXI*(ALPHA(2,2)+ALPHA(2,3))
     1     /CJ
      ALF3=ALPHA(3,2)+ALPHA(3,3)
      ALF4(N,3)=0.0
      C(M,N,1)=-2.*ALF2
      C(M,N,2)=0.0
      C(M,N,3)=2.*ALF1
      C(M,N,4)=.5*ALF2
      C(M,N,5)=0.0
      C(M,N,6)=-.5*ALF1
      C(M,N,7)=0.0
      C(M,N,8)=1.5*(ALF1-ALF2)+ALF3
C     LOWER LEFT CORNER
      XXI=-.5*(3.*X(M,1)-4.*X(M,2)+X(M,3))
      YXI=-.5*(3.*Y(M,1)-4.*Y(M,2)+Y(M,3))
      XETA=-.5*(3.*X(M,1)-4.*X(M-1,1)+X(M-2,1))
      YETA=-.5*(3.*Y(M,1)-4.*Y(M-1,1)+Y(M-2,1))
      CJ=XXI*YETA-XETA*YXI
      IF(SWITCH.NE.0) GO TO 590
      CALL ALFA(M,1,3,BT,ALPHA)
      CALL ALFA(M,1,4,BT,ALPHA)
  590 CONTINUE
      ALF1=YETA*(ALPHA(1,3)+ALPHA(1,4))/CJ-XETA*(ALPHA(2,3)+ALPHA(2,4))
     1     /CJ
```

```
      ALF2=-YXI*(ALPHA(1,3)+ALPHA(1,4))/CJ+XXI*(ALPHA(2,3)+ALPHA(2,4))
     1     /CJ
      ALF3=ALPHA(3,3)+ALPHA(3,4)
      ALF4(M,4)=0.0
      C(M,1,1)=-2.*ALF2
      C(M,1,2)=0.0
      C(M,1,3)=.5*ALF1
      C(M,1,4)=.5*ALF2
      C(M,1,5)=0.0
      C(M,1,6)=-2.*ALF1
      C(M,1,7)=0.0
      C(M,1,8)=-1.5*(ALF1+ALF2)+ALF3
C     UPPER BOUNDARY
      I=1
      ICOUNT=0
      IF(IC.EQ.0) GO TO 512
      DO 2002 II=1,3
      DO 2002 JJ=1,4
      ALPHA(II,JJ)=0.0
 2002 CONTINUE
      SWITCH=0.0
      DO 2005 ICOUNT=1,N
  512 CONTINUE
      DO 520 J=2,NM1
      XXI=.5*(X(I,J+1)-X(I,J-1))
      YXI=.5*(Y(I,J+1)-Y(I,J-1))
      XETA=.5*(3.*X(I,J)-4.*X(I+1,J)+X(I+2,J))
      YETA=.5*(3.*Y(I,J)-4.*Y(I+1,J)+Y(I+2,J))
      CJ=XXI*YETA-XETA*YXI
      IF(SWITCH.NE.0.) GO TO 515
      ALPHA(3,1)=1.0
  515 CONTINUE
      ALF1=(ALPHA(1,1)*YETA-ALPHA(2,1)*XETA)/CJ
      ALF2=(-ALPHA(1,1)*YXI+ALPHA(2,1)*XXI)/CJ
      ALF3=ALPHA(3,1)
      ALF4(J,1)=0.0
      IF(J.EQ.ICOUNT) ALF4(J,1)=1.0
      C(I,J,1)=0.0
      C(I,J,2)=0.0
      C(I,J,3)=.5*ALF1
      C(I,J,4)=2.*ALF2
      C(I,J,5)=0.0
      C(I,J,6)=-.5*ALF1
      C(I,J,7)=-.5*ALF2
      C(I,J,8)=1.5*ALF2+ALF3
  520 CONTINUE
C     UPPER LEFT CORNER
      XXI=-.5*(3.*X(1,1)-4.*X(1,2)+X(1,3))
      YXI=-.5*(3.*Y(1,1)-4.*Y(1,2)+Y(1,3))
      XETA=.5*(3.*X(1,1)-4.*X(2,1)+X(3,1))
      YETA=.5*(3.*Y(1,1)-4.*Y(2,1)+Y(3,1))
      CJ=XXI*YETA-XETA*YXI
      IF(SWITCH.NE.0.) GO TO 560
      CALL ALFA(1,1,1,BT,ALPHA)
      CALL ALFA(1,1,4,BT,ALPHA)
  560 CONTINUE
      ALF1=YETA*(ALPHA(1,1)+ALPHA(1,4))/CJ-XETA*(ALPHA(2,1)+ALPHA(2,4))
     1     /CJ
```

```
      ALF2=-YXI*(ALPHA(1,1)+ALPHA(1,4))/CJ*XXI*(ALPHA(2,1)+ALPHA(2,4))
     2     /CJ
      ALF3=ALPHA(3,1)+ALPHA(3,4)
      ALF4(1,1)=0.0
      IF(ICOUNT.EQ.1) ALF4(1,1)=1.0
      C(1,1,1)=-.5*ALF2
      C(1,1,2)=0.0
      C(1,1,3)=.5*ALF1
      C(1,1,4)=2.*ALF2
      C(1,1,5)=0.0
      C(1,1,6)=-2.*ALF1
      C(1,1,7)=0.0
      C(1,1,8)=-1.5*(ALF1-ALF2)+ALF3
C     UPPER RIGHT CORNER
      XXI=.5*(3.*X(1,N)-4.*X(1,N-1)+X(1,N-2))
      YXI=.5*(3.*Y(1,N)-4.*Y(1,N-1)+Y(1,N-2))
      XETA=.5*(3.*X(1,N)-4.*X(2,N)+X(3,N))
      YETA=.5*(3.*Y(1,N)-4.*Y(2,N)+Y(3,N))
      CJ=XXI*YETA-XETA*YXI
      IF(SWITCH.NE.0.) GO TO 570
      CALL ALFA(1,N,1,BT,ALPHA)
      CALL ALFA(1,N,2,BT,ALPHA)
  570 CONTINUE
      ALF1=YETA*(ALPHA(1,1)+ALPHA(1,2))/CJ-XETA*(ALPHA(2,1)+ALPHA(2,2))
     1     /CJ
      ALF2=-YXI*(ALPHA(1,1)+ALPHA(1,2))/CJ+XXI*(ALPHA(2,1)+ALPHA(2,2))
     1     /CJ
      ALF3=ALPHA(3,1)+ALPHA(3,2)
      ALF4(1,2)=0.0
      IF(ICOUNT.EQ.N) ALF4(1,2)=1.0
      C(1,N,1)=-.5*ALF2
      C(1,N,2)=0.0
      C(1,N,3)=2.*ALF1
      C(1,N,4)=2.*ALF2
      C(1,N,5)=0.0
      C(1,N,6)=-.5*ALF1
      C(1,N,7)=0.0
      C(1,N,8)=1.5*(ALF1+ALF2)+ALF3
C*****TIMING INFO
      CALL SECOND(TIM)
      PRINT 5000,TIM
C     SUCESSIVE OVER-RELAXATION TO SOLVE FOR PHI
      DO 600 I=1,M
      DO 600 J=1,N
      PHI(I,J)=0.0
  600 CONTINUE
      IF (IC.NE.0) PHI(1,ICOUNT)=1.0
      WX=WB
      WX=1.0
      KIT10=0
      PRINT 1200
 1200 FORMAT(*0      ITERATION*,10X,*EPSCX*,13X,*SX*,12X,*SRX*)
      DO 800 MOST=1,ITA
      KIT=MOST
      SRX=0.0
      SX=0.0
      IF(IC.NE.0) GO TO 615
C     UPPER LEFT CORNER
```

```
      PHIT=(C(1,1,1)*PHI(3,1)+C(1,1,3)*PHI(1,3)+C(1,1,4)*PHI(2,1)+
     1     C(1,1,6)*PHI(1,2)+ALF4(1,1))/C(1,1,8)
      RX=PHI(1,1)-PHIT
      PHI(1,1)=PHI(1,1)-RX*WX
      SRX=SRX+RX**2
      SX=SX+PHI(1,1)**2
C     UPPER BOUNDARY
      I=1
      DO 610 J=2,NM1
      PHIT=(C(I,J,3)*PHI(I,J-1)+C(I,J,4)*PHI(I+1,J)+C(I,J,6)*PHI(I,J+1)
     1     +C(I,J,7)*PHI(I+2,J)+ALF4(J,1))/C(I,J,8)
      RX=PHI(I,J)-PHIT
      PHI(I,J)=PHI(I,J)-RX*WX
      SRX=SRX+RX**2
      SX=SX+PHI(I,J)**2
  610 CONTINUE
C     UPPER RIGHT CORNER
      PHIT=(C(1,N,1)*PHI(3,N)+C(1,N,3)*PHI(1,N-1)+C(1,N,4)*PHI(2,N)
     1     +C(1,N,6)*PHI(1,N-2)+ALF4(1,2))/C(1,N,8)
      RX=PHI(1,N)-PHIT
      PHI(1,N)=PHI(1,N)-RX*WX
      SRX=SRX+RX**2
      SX=SX+PHI(1,N)**2
  615 CONTINUE
C     LEFT BOUNDARY
      DO 630 I=2,MM1
      J=1
      PHIT=(C(I,J,1)*PHI(I-1,J)+C(I,J,4)*PHI(I+1,J)+C(I,J,6)*PHI(I,J+1)
     1     +C(I,J,7)*PHI(I,J+2)+ALF4(I,4))/C(I,J,8)
      RX=PHI(I,J)-PHIT
      PHI(I,J)=PHI(I,J)-RX*WX
      SRX=SRX+RX**2
      SX=SX+PHI(I,J)**2
C     INTERIOR POINTS
      DO 620 J=2,NM1
      FBAR=0.0
      PHIT=C(I,J,1)*PHI(I-1,J)+C(I,J,2)*PHI(I-1,J-1)+C(I,J,3)*PHI(I,J-1)
     1    +C(I,J,4)*PHI(I+1,J)+C(I,J,5)*PHI(I+1,J+1)+C(I,J,6)*PHI(I,J+1)
      PHIT=(PHIT+FBAR)/C(I,J,8)
      FBARP(I,J)=FBAR
      RX=PHI(I,J)-PHIT
      PHI(I,J)=PHI(I,J)-RX*WX
      SRX=SRX+RX**2
      SX=SX+PHI(I,J)**2
  620 CONTINUE
C     RIGHT BOUNDARY
      J=N
      PHIT=(C(I,J,1)*PHI(I-1,J)+C(I,J,3)*PHI(I,J-1)+C(I,J,4)*PHI(I+1,J)
     1     +C(I,J,7)*PHI(I,J-2)+ALF4(I,2))/C(I,J,8)
      RX=PHI(I,J)-PHIT
      PHI(I,J)=PHI(I,J)-RX*WX
      SRX=SRX+RX**2
      SX=SX+PHI(I,J)**2
  630 CONTINUE
C     LOWER LEFT CORNER
      PHIT=(C(M,1,1)*PHI(M-1,1)+C(M,1,3)*PHI(M,3)+C(M,1,4)*PHI(M-2,1)
     1     +C(M,1,6)*PHI(M,2)+ALF4(M,4))/C(M,1,8)
      RX=PHI(M,1)-PHIT
```

```
      PHI(M,1)=PHI(M,1)-RX*WX
      SRX=SRX+RX**2
      SX=SX+PHI(M,1)**2
C     LOWER BOUNDARY
      I=M
      DO 640 J=2,NM1
      PHIT=(C(I,J,1)*PHI(I-1,J)+C(I,J,3)*PHI(I,J-1)+C(I,J,6)*PHI(I,J+1)
     1     +C(I,J,7)*PHI(I-2,J)+ALF4(J,3))/C(I,J,8)
      RX=PHI(I,J)-PHIT
      PHI(I,J)=PHI(I,J)-RX*WX
      SRX=SRX+RX**2
      SX=SX+PHI(I,J)**2
  640 CONTINUE
C     LOWER RIGHT CORNER
      PHIT=(C(M,N,1)*PHI(M-1,N)+C(M,N,3)*PHI(M,N-1)+C(M,N,4)*PHI(M-2,N)
     1     +C(M,N,6)*PHI(M,N-2)+ALF4(N,3))/C(M,N,8)
      RX=PHI(M,N)-PHIT
      PHI(M,N)=PHI(M,N)-RX*WX
      SRX=SRX+RX**2
      SX=SX+PHI(M,N)**2
      IF(SX.EQ.0.0) GO TO 730
      IF(KIT.EQ.1) SPRX=SRX
      EPSCX=SQRT(SRX/SX)
      IF(EPSCX.GE.20.) STOP
      IF(EPSCX.LE.EPS) GO TO 730
      ETAX=SQRT(SRX/SPRX)
      ELX=(WX+ETAX-1.0)/(WX*SQRT(ETAX))
      IF(ABS(ELX)-1.0)680,680,660
  660 WAX=WX
      GO TO 690
  680 WAX=2.0/(1.0+SQRT(1.0-ELX**2))-WO
  690 WX=RHO*WAX+(1.0-RHO)*WX
      WX=1.0
      IF(WX.LT.1.0) WX=1.0
      SPRX=SRX
      KIT10=KIT10+1
      IF(KIT10.LT.20) GO TO 700
      PRINT 1210,KIT,EPSCX,SX,SRX,WX
 1210 FORMAT(I15,4E15.7)
      KIT10=0
  700 CONTINUE
C     CALCULATE BY ROW FROM RIGHT TO LEFT AND BOTTOM TO TOP
C     LOWER BOUNDARY
      I=M
      DO 750 L=2,NM1
      J=N+1-L
      PHIT=(C(I,J,1)*PHI(I-1,J)+C(I,J,3)*PHI(I,J-1)+C(I,J,6)*PHI(I,J+1)
     1     +C(I,J,7)*PHI(I-2,J)+ALF4(J,3))/C(I,J,8)
      RX=PHI(I,J)-PHIT
      PHI(I,J)=PHI(I,J)-RX*WX
  750 CONTINUE
C     LOWER LEFT CORNER
      PHIT=(C(M,1,1)*PHI(M-1,1)+C(M,1,3)*PHI(M,3)+C(M,1,4)*PHI(M-2,1)
     1     +C(M,1,6)*PHI(M,2)+ALF4(M,4))/C(M,1,8)
      RX=PHI(M,1)-PHIT
      PHI(M,1)=PHI(M,1)-RX*WX
      DO 770 K=2,MM1
      I=M+1-K
```

```
C       RIGHT BOUNDARY
        J=N
        PHIT=(C(I,J,1)*PHI(I-1,J)+C(I,J,3)*PHI(I,J-1)+C(I,J,4)*PHI(I+1,J)
       1     +C(I,J,7)*PHI(I,J-2)+ALF4(I,2))/C(I,J,8)
        RX=PHI(I,J)-PHIT
        PHI(I,J)=PHI(I,J)-RX*WX
C       INTERIOR POINTS
        DO 760 L=2,NM1
        J=N+1-L
        FBAR=0.0
        PHIT=C(I,J,1)*PHI(I-1,J)+C(I,J,2)*PHI(I-1,J-1)+C(I,J,3)*PHI(I,J-1)
       1    +C(I,J,4)*PHI(I+1,J)+C(I,J,5)*PHI(I+1,J+1)+C(I,J,6)*PHI(I,J+1)
        PHIT=(PHIT+FBAR)/C(I,J,8)
        FBARP(I,J)=FBAR
        RX=PHI(I,J)-PHIT
        PHI(I,J)=PHI(I,J)-RX*WX
  760 CONTINUE
C       LEFT BOUNDARY
        J=1
        PHIT=(C(I,J,1)*PHI(I-1,J)+C(I,J,4)*PHI(I+1,J)+C(I,J,6)*PHI(I,J+1)
       1     +C(I,J,7)*PHI(I,J+2)+ALF4(I,4))/C(I,J,8)
        RX=PHI(I,J)-PHIT
        PHI(I,J)=PHI(I,J)-RX*WX
  770 CONTINUE
        IF(IC.NE.0) GO TO 800
C       UPPER RIGHT CORNER
        PHIT=(C(1,N,1)*PHI(3,N)+C(1,N,3)*PHI(1,N-1)+C(1,N,4)*PHI(2,N)
       1     +C(1,N,6)*PHI(1,N-2)+ALF4(1,2))/C(1,N,8)
        RX=PHI(1,N)-PHIT
        PHI(1,N)=PHI(1,N)-RX*WX
C       UPPER BOUNDARY
        I=1
        DO 780 L=2,NM1
        J=N+1-L
        PHIT=(C(I,J,3)*PHI(I,J-1)+C(I,J,4)*PHI(I+1,J)+C(I,J,6)*PHI(I,J+1)
       1     +C(I,J,7)*PHI(I+2,J)+ALF4(J,1))/C(I,J,8)
        RX=PHI(I,J)-PHIT
        PHI(I,J)=PHI(I,J)-RX*WX
  780 CONTINUE
  800 CONTINUE
        PRINT 1110,KIT,EPSCX,SX,SRX
  710 DO 720 I=1,M
        PRINT 1100,(PHI(I,J),J=1,N)
  720 CONTINUE
C*****TIMING INFO
        CALL SECOND(TIM)
        PRINT 5000,TIM
        GO TO 810
  730 PRINT 1120,KIT
        PRINT 1140,EPSCX,SX,RX,WX
C*****TIMING INFO
        CALL SECOND(TIM)
        PRINT 5000,TIM
        DO 808 I=1,M
        PRINT 1100,(PHI(I,J),J=1,N)
  808 CONTINUE
  810 CONTINUE
        I=1
```

```
      DO 2001 J=2,NM1
      XXI=.5*(X(I,J+1)-X(I,J-1))
      YXI=.5*(Y(I,J+1)-Y(I,J-1))
      XETA=.5*(3.*X(I,J)-4.*X(I+1,J)+X(I+2,J))
      YETA=.5*(3.*Y(I,J)-4.*Y(I+1,J)+Y(I+2,J))
      CJ=XXI*YETA-XETA*YXI
      ALF1=-XETA/CJ
      ALF2= XXI/CJ
      PHIXI=0.5*(PHI(1,J+1)-PHI(1,J-1))
      PHIETA= 0.5*(3.*PHI(1,J)-4.*PHI(2,J)+PHI(3,J))
      CV(J)=ALF1*PHIXI + ALF2 *PHIETA
 2001 CONTINUE
      XXI=-.5*(3.*X(1,1)-4.*X(1,2)+X(1,3))
      YXI=-.5*(3.*Y(1,1)-4.*Y(1,2)+Y(1,3))
      XETA=.5*(3.*X(1,1)-4.*X(2,1)+X(3,1))
      YETA=.5*(3.*Y(1,1)-4.*Y(2,1)+Y(3,1))
      CJ=XXI*YETA-XETA*YXI
      J=1
      ALF1=-XETA/CJ
      ALF2= XXI/CJ
      PHIXI= -0.5*(3.*PHI(1,J)-4.*PHI(2,J)+PHI(3,J))
      PHIETA= 0.5*(3.*PHI(1,J)-4.*PHI(2,J)+PHI(3,J))
      CV(J)=ALF1*PHIXI + ALF2 *PHIETA
      XXI=.5*(3.*X(1,N)-4.*X(1,N-1)+X(1,N-2))
      YXI=.5*(3.*Y(1,N)-4.*Y(1,N-1)+Y(1,N-2))
      XETA=.5*(3.*X(1,N)-4.*X(2,N)+X(3,N))
      YETA=.5*(3.*Y(1,N)-4.*Y(2,N)+Y(3,N))
      CJ=XXI*YETA-XETA*YXI
      J=N
      ALF1=-XETA/CJ
      ALF2= XXI/CJ
      PHIXI=  0.5*(3.*PHI(1,J)-4.*PHI(2,J)+PHI(3,J))
      PHIETA= 0.5*(3.*PHI(1,J)-4.*PHI(2,J)+PHI(3,J))
      CV(J)=ALF1*PHIXI + ALF2 *PHIETA
      DO 2003  J=1,N
      F(J,ICOUNT)=CV(J)
 2003 CONTINUE
      DO 2004 II=1,3
      ALPHA(II,1)=0.
 2004 CONTINUE
 2005 CONTINUE
      DO 2006 I=1,N
      DO 2006 J=1,N
      EVAL(I,J)=F(I,J)
 2006 CONTINUE
      CALL EIGEN(N,EVAL,EVI,EVEC,50,3,0,1,NDIM)
      DO 2008 I=1,N
      NVAL (I)=I
      EIGVAL(I)=   EVAL(I,I)
 2008 CONTINUE
      DO 375 I=1,N
      K=I
      DO 374 J=K,N
      IF (EIGVAL(I)-EIGVAL(J)) 374,374,373
  373 XTEMP=EIGVAL(J)
      II=NVAL(J)
      EIGVAL(J)=EIGVAL(I)
      NVAL(J)=NVAL(I)
```

```
      EIGVAL(I)=XTEMP
      NVAL(I)=II
  374 CONTINUE
  375 CONTINUE
      PRINT 400,ITITLE
  400 FORMAT (1H1,12A6/)
      PRINT 401
  401 FORMAT (77H EIGENVALUES AND EIGENVECTORS ASSOCIATED WITH INFLUENCE
     1 COEFFICIENT SOLUTIONS)
      DO 376 I=1,N
      PRINT 402,I,EIGVAL(I)
  402 FORMAT (6H MODE ,I3,14H   EIGENVALUE ,E15.8)
      K=NVAL(I)
      PRINT 202,(EVEC(J,K),J=1,N)
  376 CONTINUE
C     AUXILARY EIGENVECTORS DETERMINED
      GO TO 10
 1100 FORMAT(8E15.7)
 1110 FORMAT(*1SOLUTION DID NOT CONVERGE FOR COEFFICIENTS*/,
     1       * AFTER *,I5,* ITERATIONS   EPSCX= *,E15.7,
     2       *   SX= *,E15.7,*   SRX= *,E15.7/)
 1120 FORMAT(*1COEFFICIENT SOLUTION CONVERGED AFTER ITERATION*,I5)
 1130 FORMAT(*1JACOBIAN*)
 1140 FORMAT(* EPSCX =*,E15.7,*   SX =*,E15.7,*   RX =*,E15.7,
     1       *   WX =*,E15.7/)
 1160 FORMAT(*0ALPHA(I,J)*)
      END
```

```
      SUBROUTINE ALFA(I,J,K,BT,ALPHA)
      DIMENSION ALPHA(3,4),X(40,24),Y(40,24)
      COMMON AE,BE,CE,DE,EE,SINT,COST,HO,X,Y
      ETA=X(I,J)*SINT+Y(I,J)*COST
      IF(BT.EQ.-1.0) GO TO 30
      IF(ETA.GT.-HO) GO TO 20
   10 ALPHA(1,K)=-COST
      ALPHA(2,K)=SINT
      ALPHA(3,K)=0.0
      IF(J.EQ.1) RETURN
      ALPHA(1,K)=COST
      ALPHA(2,K)=-SINT
      RETURN
   20 FX=2.0*AE*X(I,J)+BE*Y(I,J)+DE
      FY=BE*X(I,J)+2.0*CE*Y(I,J)+EE
      RT=SQRT(FX**2+FY**2)
      ALPHA(1,K)=FX/RT
      ALPHA(2,K)=FY/RT
      ALPHA(3,K)=0.0
      RETURN
   30 IF(ETA+HO)20,10,10
      END
```

```
      SUBROUTINE EIGEN(N,B,TI,T,MAXIT,NDEC,N1OPT,N2OPT,NDIM)
C     SUBROUTINE FOR GENERATING THE EIGENVALUES AND EIGENVECTORS
C     OF A REAL SYMMETRIC OR NON-SYMMETRIC MATRIX.
C     THIS PROGRAM GENERATES THE EIGENVALUE MATRIX(REAL OR COMPLEX),
C     AND AS OPTIONS, THE EIGENVECTOR MATRIX AND ITS INVERSE.
C       THE CALL FOR THIS SUBROUTINE IS AS FOLLOWS.
C     CALL EIGEN (N,B,TI,T,MAXIT,NDEC,N1OPT,N2OPT,NDIM)
C       WHERE N IS THE ORDER OF THE MATRIX
C             B IS THE MATRIX WHOSE EIGENVALUES ARE DESIRED
C            TI IS THE INVERSE OF THE EIGENVECTOR MATRIX
C             T IS THE EIGENVECTOR MATRIX
C         MAXIT IS MAX NO. OF ITERATIONS FOR GENERATING EIGENVALUES
C        NDEC IS THE NUMBER OF TIMES RESULT IS REFINED
C         N1OPT IS 1 IF OPTION =1 IS DESIRED, OTHERWISE 0,
C     OPTION =1 PROVIDES FOR GENERATING THE EIGENVECTOR MATRIX INVERSE
C         N2OPT IS 1 IF OPTION =2 IS DESIRED, OTHERWISE 0,
C     OPTION =2 PROVIDES FOR GENERATING THE EIGENVECTOR MATRIX
C          NDIM IS DIMENSIONED NO. OF ROWS OF MATRIX (B)
C       THE ORGINAL MATRIX B IS LOST DURING THE COMPUTATIONS AND IS
C     REPLACED BY THE EIGENVALUE MATRIX.
      DIMENSION B(1),TI(1),T(1)
C     INITIALIZE COUNTERS FOR NO. OF ITERATIONS AND YR,YS REDUCTIONS
      IT=0
      NTIMES=0
      ANORM=0.0
      DO 1100 I=1,N
      DO 1100 J=1,N
      IJ=(J-1)*NDIM+I
 1100 ANORM=ANORM+B(IJ)**2
      ANORM=SQRTF(ANORM)
      DO 1101 I=1,N
      DO 1101 J=1,N
      IJ=(J-1)*NDIM+I
 1101 B(IJ)=B(IJ)/ANORM
C     FORM IDENTITY MATRIX IN TI LOCATION IF OPTION 1 IS DESIRED
 1000 IF(N1OPT)1010,1010,1001
 1001 DO 1003 I=1,N
      II = (I-1)*NDIM+I
      DO 1002 J=1,N
      IJ = (J-1)*NDIM+I
 1002 TI(IJ) = 0.
 1003 TI(II) = 1.0
C     FORM IDENTITY MATRIX IN T LOCATION IF OPTION 2 DESIRED
 1010 IF(N2OPT)1020,1020,1011
 1011 DO 1013 I=1,N
      II = (I-1)*NDIM+I
      DO 1012 J=1,N
      IJ = (J-1)*NDIM+I
 1012 T(IJ) = 0.
 1013 T(II) = 1.0
 1020 CONTINUE
      YR=10.0E-7
      YS=10.0E-7
   96 NQ=N-1
      SUM=10.0E20
   97 TAU=0.0
      EN=0.0
```

```
      DO 1 I=1,NO
      JO=I+1
      DO 1 J=JO,N
      IJ = (J-1)*NDIM+I
      JI = (I-1)*NDIM+J
    1 TAU = TAU+B(IJ)**2+B(JI)**2
      DO 2 I=1,N
      II = (I-1)*NDIM+I
      TE = B(II)
    2 EN=EN+TE**2
    4 EN=EN+TAU
    5 DELN=SUM-EN
    6 IF(DELN)8,8,7
    7 SUM=EN
      IT=IT+1
      IF(MAXIT-IT)120,120,10
    8 CONTINUE
      IF(NDEC-NTIMES)120,120,9
    9 YR=YR/100.0
      YS=YS/100.0
      NTIMES=NTIMES+1
      IT=IT+1
   10 DO 98 K=1,NO
      KK = (K-1)*NDIM+K
      KO=K+1
   11 DO 98 M=KO,N
      MM = (M-1)*NDIM+M
      KM = (M-1)*NDIM+K
      MK = (K-1)*NDIM+M
      H=0.0
      G=0.0
      HJ=0.0
   12 DO 24 I=1,N
   13 IF(I-K)14,24,14
   14 IF(I-M)15,24,15
   15 IK = (K-1)*NDIM+I
      KI = (I-1)*NDIM+K
      IM = (M-1)*NDIM+I
      MI = (I-1)*NDIM+M
      BO = B(IK)
   16 BR = B(KI)
   17 BQ = B(IM)
   18 BS = B(MI)
   19 H=H+BR*BS-BO*BQ
   20 TEP=BO*BO+BS*BS
   21 TEM=BR*BR+BQ*BQ
   22 G=G+TEP+TEM
   23 HJ=HJ-TEP+TEM
   24 CONTINUE
   25 H=2.0*H
      D = B(KK)-B(MM)
      TEP = B(KM)
      TEM = B(MK)
      C=TEP+TEM
      E=TEP-TEM
   26 IF(ABSF(C)-YR)27,27,30
   27 CC=1.0
   28 SS=0.0
```

```
   29 GO TO 39
   30 BY=D/C
   31 IF(BY)400,401,401
  400 SIG=-1.0
      GO TO 32
  401 SIG =1.0
   32 COT=BY+(SIG*SQRTF(BY*BY+1.0))
   33 SS=SIG/SQRTF(COT*COT+1.0)
   34 CC=SS*COT
   35 TEP=CC*CC-SS*SS
   36 TEM=2.0*SS*CC
   37 D=D*TEP+C*TEM
   38 H=H*TEP-HJ*TEM
   39 CONTINUE
   40 ED=2.0*E*D
   41 EDH=ED-H
   42 DEN=G+2.0*(E*E+D*D)
   43 TEE=EDH/(DEN*DEN)
   75 CONTINUE
  205 IF(ABSF(TEE)-YS)44,44,46
   44 CH=1.0
   45 SH=0.0
      GO TO 48
   46 CH=1.0/SQRTF(1.0-TEE*TEE)
   47 SH=TEE*CH
   48 C1=CH*CC-SH*SS
   49 C2=CH*CC+SH*SS
   50 S1=CH*SS+SH*CC
   51 S2=-CH*SS+SH*CC
   52 CONTINUE
   53 IF(S1)55,54,55
   54 IF(S2)55,98,55
   55 DO 59 J=1,N
      KJ = (J-1)*NDIM+K
      MJ = (J-1)*NDIM+M
   56 BO = B(KJ)
   57 BR = B(MJ)
   58 B(KJ) = C1*BO+S1*BR
   59 B(MJ) = S2*BO+C2*BR
   60 DO 66 J=1,N
      JK = (K-1)*NDIM+J
      JM = (M-1)*NDIM+J
   61 BO = B(JK)
   62 BR = B(JM)
   65 B(JK) = BO*C2-BR*S2
   66 B(JM) = -BO*S1+BR*C1
 1070 IF(N10PT)1075,1075,1071
 1071 DO 1072 J=1,N
      KJ = (J-1)*NDIM+K
      MJ = (J-1)*NDIM+M
      BQ = TI(KJ)
      BS = TI(MJ)
      TI(KJ) = C1*BQ+S1*BS
 1072 TI(MJ) = S2*BQ+C2*BS
 1075 IF(N20PT)98,98,1076
 1076 DO 1077 J=1,N
      JK = (K-1)*NDIM+J
      JM = (M-1)*NDIM+J
```

```
      BO = T(JK)
      BR = T(JM)
      T(JK) = BO*C2-BR*S2
1077  T(JM) = -BO*S1+BR*C1
   98 CONTINUE
      GO TO 97
  120 DO 1102 I=1,N
      DO 1102 J=1,N
      IJ=(J-1)*NDIM+I
1102  B(IJ)=B(IJ)*ANORM
      IF (N2OPT) 1107,1107,1103
1103  DO 1106 J=1,N
      ANORM=0.0
      DO 1104 I=1,N
      IJ=(J-1)*NDIM+I
1104  ANORM=ANORM+T(IJ)**2
      ANORM=SQRTF(ANORM)
      DO 1105 I=1,N
      IJ=(J-1)*NDIM+I
1105  T(IJ)=T(IJ)/ANORM
1106  CONTINUE
1107  RETURN
      END
```